The Pennsylvania State University

Department of Civil and Environmental Engineering

SEISMIC PERFORMANCE OF BASE ISOLATED BUILDINGS AND STRATEGIES TO MITIGATE VERTICAL ACCELERATION DEMANDS

A Thesis in

Civil Engineering

by

Bach Xuan Vu

Submitted in Partial Fulfillment

of the Requirements

for the Degree of

Master of Science

August 2012

The thesis of Bach Xuan Vu was reviewed and approved* by the following:

Gordon Warn
Assistant Professor of Civil Engineering
Thesis Advisor

Swagata Banerjee Basu
Assistant Professor of Civil Engineering

Ali M. Memari
Bernard and Henrietta Hankin Chair in Residential Building Construction Professor of Architectural Engineering

Peggy Johnson
Professor of Civil Engineering
Head of the Department of Civil and Environmental Engineering

*Signatures are on file in the Graduate School.

Abstract

Elastomeric bearing constructed of rubber layers bonded to intermediate steel shim plates is a seismic isolation device used for protecting a structure against earthquake ground shaking. The rubber layers provide the low lateral stiffness required to shift the period whereas the close spacing of the intermediate steel shim plates provides a vertical stiffness that is several thousand times larger than a horizontal stiffness. However, the low vertical isolation frequency can align with the dominant frequency content of the vertical spectrum leading to significant amplification of accelerations. An analytical study was conducted to investigate the influence of the vertical component of ground shaking on the performance of nonstructural systems within multi-story seismically isolated buildings. The research focuses on two dimensional analytical models of 3 and 9-story frames. Three model configurations are explored namely: frames with conventional base isolation, frames with base isolation and viscous dampers, and lastly frames with base isolation and column isolators. Fragility curves are used to assess damage to ceiling systems in both frames. Results from analytical analyses suggests that damage to ceiling systems might be mitigated in low-rise structure using moderate shape factor elastomeric bearings and supplemental damping, and in middle rise structure using high shape factor base bearings and column isolators.

Table of Contents

Chapter 1

Introduction

1.1 Background and Motivation

Seismic isolation is a technique used to protect structures and nonstructural systems from the damaging effect of horizontal earthquake ground motion. This is accomplished by decoupling the superstructure from the substructure using isolation bearings with low lateral stiffness. The low lateral stiffness is required to shift the period of the structure into the long period range, e.g., 2.5s to 4s. This period shift translates into reduced spectral acceleration demands as illustrated by the shaded region on the elastic response spectra shown in Fig. 1.1a (generated using the recorded earthquake ground motions detailed in Chapter 3). The period shift, however, does result in increased displacement demands concentrated at the isolation interface that must be accommodated by the seismic isolation bearings. Seismic isolation bearings fall into two general categories, namely: (1) elastomeric and (2) sliding. Each type has low lateral stiffness to achieve the desired period shift and a large vertical stiffness to support the gravity and vertical forces imposed on during service and seismic loading, respectively.

For elastomeric bearing, the total thickness of rubber provides the low lateral stiffness whereas closely spaced steel shim plates provide a vertical stiffness that is several thousand times larger than the horizontal stiffness. Consequently, the vertical isolation frequencies, typically ranging from 0.03 to 0.15 seconds, can align with the dominant frequency content of the vertical spectrum leading to significant amplification of accelerations. For sliding bearings, the low lateral stiffness is achieved using bearing material such as polytetrafluoroethylene (PTFE) type material mated to polished stainless steel providing a low sliding coefficient of friction ranging from 0.07 to 0.18 (Mohka et al. 1990a, b) with values as low as 0.03 (EPS 2012). However, the materials used to construct sliding bearings produce a large vertical stiffness and thus a low vertical isolation period, typically around 0.03 seconds (EPS 2012).

The short vertical isolation period produced by typical elastomeric and sliding isolation bearing, e.g., 0.03 to 0.15 seconds, can align with dominant frequency content of vertical spectrum as shown by the shaded region plotted in Fig. 1.1b superimposed on spectra generated using the vertical components of recorded earthquake ground motions. Therefore, bearings

widely used for seismic isolation provide isolation only in the horizontal direction and are not designed to protect against vertical ground shaking.

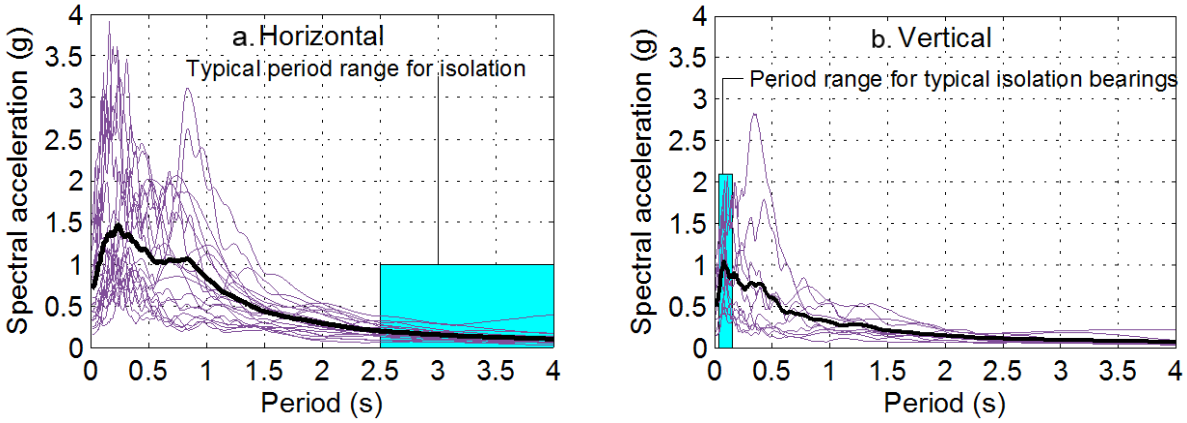

Figure 1.1. Elastic, 5% damping, earthquake response spectra from Bin 1: (a) horizontal component; (b) vertical component

Observations from reconnaissance following the 1995 Kobe earthquake in Japan and the 1994 Northridge earthquake in the United States indicate that damage to structural and non-structural components in fixed-base structure were due to demands imposed on these elements from the vertical components of earthquake ground shaking (Papazoglou and Elnashai 1996). Other studies (Kageyama et al. 2004; Yoo et al. 1997) suggest the larger vertical stiffness provided by isolation systems composed of elastomeric bearings could result in acceleration demands that are greater than those in an equivalent non-isolated structure. This suggests structures isolated on bearings with large vertical stiffness could sustain damage to structural and non-structural components due to the vertical component of ground motion.

Recently, two independent test programs on full scale isolated buildings with weights of 5,000-10,000 kN have been conducted at the National Institute for Earth Science and Disaster Prevention (NIED) E-Defense shaking table of Japan (Sato et al. 2010; Ryan et al. 2012). While the influence of vertical excitation has not yet been reported from the Sato et al. tests (2010), Ryan et al. (2012) observed damage to suspended ceilings. Observed damage included ceiling panels falling and in the most extreme cases localized failures of the ceiling grid support system (Soroushian et al. 2012).

1.2 Objective

To date, no comprehensive analytical or experimental study has been conducted to understand the impact of the vertical component of ground shaking on the performance of nonstructural systems within multi-story seismically isolated buildings. Yet, damage to these systems could adversely affect the post event functionality of critical facilities such as hospitals and emergency centers for which seismic isolation is typically employed (Sato 2011).

The first objective of this study is to investigate how the isolation system's properties, specifically vertical stiffness and vertical damping, affect vertical acceleration demands in the upper levels of the building and the probability of damage to suspended ceiling systems. Suspended ceiling systems were chosen as the nonstructural component because damage to this nonstructural system was observed during recent full scale testing of a base isolated structure (Soroushian et al. 2012). Furthermore, seismic fragility data for suspended ceiling systems is available in the literature (Badillo et al. 2006) though a number of assumptions are required to apply the data to this study as described in subsequent sections.

Secondly, past efforts to achieve three-dimensional isolation have been investigated as will be discussed in the literature review section of this proposal (Tajirian et al. 1990; Huffmann 1984; Kageyama et al 2002 and Takahashi et al. 2008). However, each of these strategies has concentrated on the horizontal and vertical flexibility at the base of the structures. In structures where the center of mass is elevated above the plane of isolation, this vertical flexibility translates into reduced rocking periods of vibration that increases the participation of rocking response, in turn increasing horizontal and vertical acceleration demands in the upper levels of the building. Furthermore, decreasing the vertical stiffness of the isolation device to the point of achieving vertical isolation typically requires using a device with limited stability and is difficult to achieve in practice. Rather than concentrating vertical flexibility at the base to achieve three-dimensional isolation, a strategy is proposed in this study to distribute the vertical flexibility up the height of the building. One possibility to achieve this “distributed vertical flexibility” could be through the use of elastomeric laminated bearings that are laterally restrained, similar to pot bearings, installed at various locations up the height of the building. The effect of supplemental vertical damping located at the base of the building will also be explored.

1.3 Research Significance

First, this study offers a systematic analytical parametric study of the influence of bearing shape factor on vertical acceleration demands in multi-story seismically isolated frames. Secondly, this study proposes a use of non-structural fragility data to estimate the likelihood of damage to non-structural components (namely suspended ceiling systems) for evaluation of various systems. Finally, this study provides a development and demonstration of the vertically distributed flexibility concept.

1.4 Scope of Research

This research is limited to analytical studies of two-dimensional, three-story and nine-story models based on the SAC Los Angeles buildings from Gupta and Krawinkler (1999). There are three system configurations considered in this research. The first is structures with conventional base isolation; the second is structures with conventional base isolation and supplemental vertical viscous dampers located at the plane of base isolation. The third configuration is base isolation with vertically distributed flexibility. Finally, fragility curves adapted from Badillo et al. (2006) were used to assess damage due to vertical component of earthquake excitation to ceiling systems and to evaluate the three configurations.

1.5 Research Plan

The objectives of this research will be achieved through the following research plan consisting of four tasks:

1. Perform an analytical parametric study to systematically investigate the influence of the isolation system properties, specifically vertical stiffness, on the vertical acceleration demands in the upper stories of seismically isolated buildings.
2. Assess the probability of damage to suspended ceilings in the upper stories of seismically isolated buildings using seismic fragility data.
3. Explore new systems to minimize damage to suspended ceiling systems in seismically isolated buildings.
4. Using fragility curves to verify the efficacy of the new systems through an analytical study.

1.6 Organization of thesis proposal

This proposal is organized into the following seven sections: (1) Introduction; (2) Background information and literature review; (3) Research approach; (4) Analytical results; (5) Summary and conclusions; (6) References; (7) Appendices.

Chapter 2

Background information and literature review

2.1 General

This chapter provides background information and a review of literature pertaining to seismic isolation and elastomeric bearings. Additionally, seismic fragility testing of suspended ceiling systems will be reviewed as data from an experimental test program by Badillo et al. (2006) was adapted for this study.

2.2 Background theory

Figure 2.1 illustrates the concept of isolation using a typical design earthquake response spectrum. A fixed base structure that would be a candidate for seismic isolation will have a short fundamental period, e.g., smaller than 1 second corresponding to a region of the spectrum where there is significant amplification of spectral acceleration demands. Seismic isolation is achieved by shifting the fundamental period of the structure into the long period range, e.g., 2.5s to 4s, with the aim of reducing spectral acceleration demands below the peak ground acceleration. The reduced demands allow the superstructure to be designed to remain elastic, or nearly elastic, following the design level event. Furthermore, the reduced demands minimize the likelihood of damage to displacement sensitive and acceleration sensitive equipment, nonstructural components and contents. The period shift, however, does result in increased displacement demands concentrated at the isolation interface that must be accommodated by the seismic isolation devices. The simultaneous reduction in horizontal acceleration and inter-story drift demands achieved with seismic isolation makes it one of the most effective strategies for protection against horizontal ground shaking.

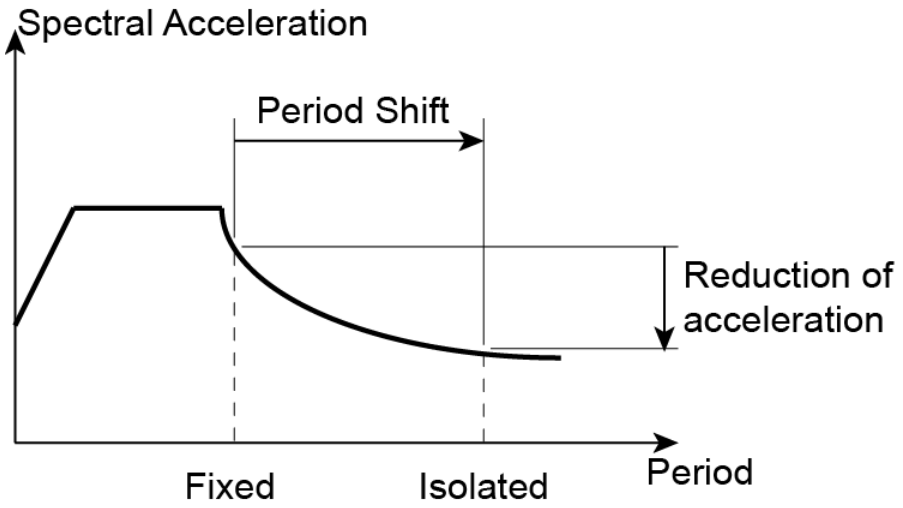

Figure 2.1. Illustration of the concept of isolation on a typical earthquake design response spectrum

Sliding bearings have very large vertical stiffness that cannot easily be modified due to the materials and methods used to construct these devices. In contrast, the vertical stiffness of the elastomeric bearing can be varied widely by modifying the number and proportions of the individual rubber layers. For this reason, the remainder of this study will focus on elastomeric bearings.

2.3 Elastomeric bearings

Elastomeric bearings are constructed of alternating rubber layers bonded to intermediate reinforcing plates that are typically steel as illustrated by the schematic of a deformed bearing shown in Fig. 2.2. The total thickness of rubber (T_r) provides the low horizontal stiffness need to achieve the period shift whereas the spacing of the steel shim plates controls the vertical stiffness of the bearing for a given shear modulus (G) and bonded rubber area (A_b).

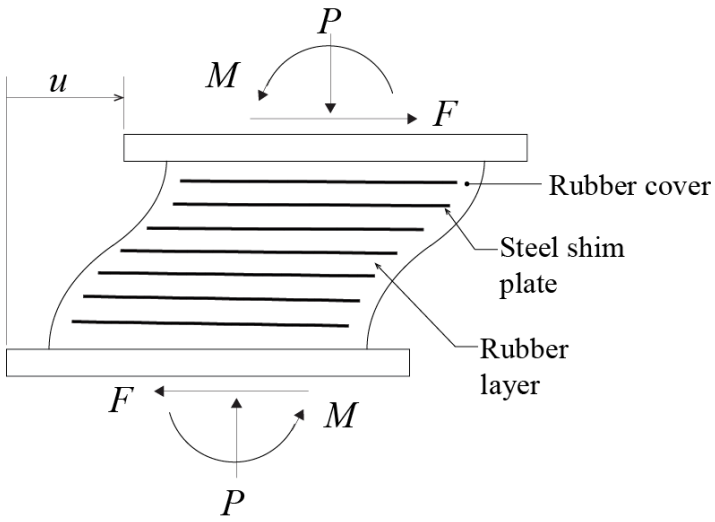

Figure 2.2. Schematic of an elastomeric bearing in the laterally deformed configuration

2.3.1 Mechanical behavior

The horizontal stiffness of an elastomeric bearing (Kelly 1997) is calculated as:

$$K_h = \frac{G_{eff} A_b}{T_r} \tag{2.1}$$

where G_{eff} is the effective shear modulus, A_b is the bonded rubber area of the bearing. The total thickness of rubber (T_r) is equal the number of rubber layers (n) times the individual rubber layer thickness (t_r). The vertical stiffness of an elastomeric bearing (Kelly 1997) is calculated according to:

$$K_v = \frac{E_c A_b}{T_r} \tag{2.2}$$

where E_c is the instantaneous compression modulus of the rubber-steel composite.

The compression modulus (E_c) for an individual rubber layer is controlled by the shape and thickness of the individual rubber layers. For a solid circular rubber pad, the compression modulus assuming incompressible material (Chalhoub and Kelly 1990) is:

$$E_c = 6G_{eff} S^2 \tag{2.3}$$

The shape factor S (Kelly 1997) is a dimensionless geometric parameter defined as:

$$S = \frac{\text{Loaded area}}{\text{Area free to bulge}} \tag{2.4}$$

where the loaded area and area free to bulge are illustrated in Fig. 2.3. For a circular pad with bonded diameter D, and thickness t_r, the shape factor is:

$$S = \frac{D}{4t_r} \tag{2.5}$$

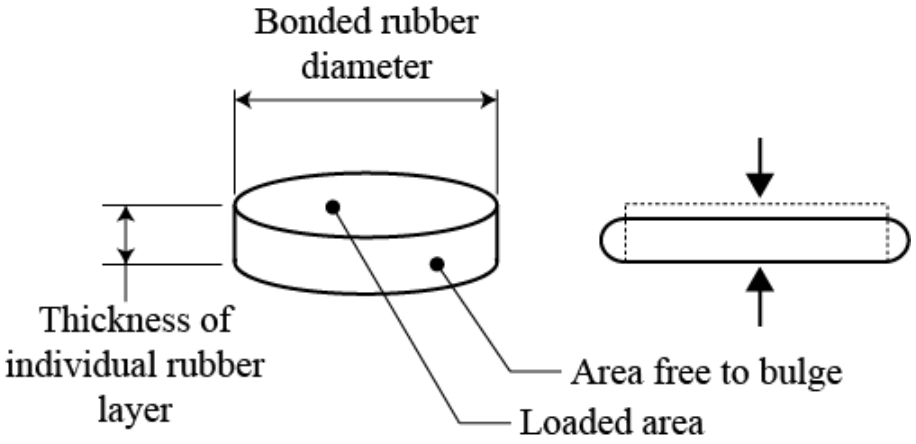

Figure 2.3. Illustration of loaded area and area free to bulge for individual rubber layer

Inspection of Eq. 2.1, 2.2 and 2.3 reveals that the horizontal and vertical stiffness of a solid circular elastomeric bearing are related as:

$$\frac{K_v}{K_h} = 6S^2 \tag{2.6}$$

Elastomeric seismic isolation bearings are typically detailed with shape factors ranging from 15 to 25 (HITEC1998a, b). According to Eq. 2.6, the resulting vertical stiffness for shape factors in this range is several thousand times larger than the horizontal stiffness. While the large vertical stiffness minimizes the vertical deformation, it translates into a low vertical period leading to significant amplification of the vertical acceleration demands as illustrated in Fig 1.1b. Therefore, an isolation system composed of elastomeric bearing with high shape factor (15-25) provides isolation only in the horizontal direction.

2.3.2 Stability of elastomeric bearings

The isolation devices are typically installed between the superstructure and foundation (substructure). Therefore, these devices must be designed to remain stable for service level loading and seismic loading. Elastomeric bearings, however, have limited stability for the lateral un-deformed configuration (service) that is reduced further with lateral displacement (seismic) so that stability is an important consideration in the design of an isolation system composed of elastomeric bearings.

The vertical critical load in the laterally un-deformed configuration P_{cro} (Haringx 1948; Haringx 1949 a, b; Gent 1964; Derham and Thomas 1981) is calculated as:

$$P_{cro} = \frac{\sqrt{(P_S^2 + 4P_S P_E)} - P_S}{2} \tag{2.7}$$

where P_S is the shear rigidity equal to the shear modulus (G_{eff}) times an effective shear area (A_s) and P_E is the Euler buckling load. The Euler buckling load is calculated as $P_E = \pi^2 E_r I_s / h^2$, in which E_r is the bending modulus. For a circular bearing, E_r (Kelly 1997) is equal to the compression modulus (E_c) divided by 3. An effective area A_s and bending moment of inertia, I_s, is used in the critical load calculation to account for the composite construction of the bearing (Kelly 1997) where $A_s = A_b(h/T_r)$ and $I_s = I(h/T_r)$ where h is the height of the combine of rubber and steel plates and I is the moment of inertia of bearing.

According to Guide Specification for Seismic Isolation Design (AASHTO 2010), the vertical load capacity (P_{cro}) of the bearing must satisfy the following inequality:

$$\frac{P_{cro}}{P_D + P_L} \geq 3 \tag{2.8}$$

During earthquake motion, the bearings will be subjected to simultaneous vertical compression load and lateral displacement as illustrated in Fig. 2.2. The overlapping area method (Buckle and Liu 1994) is used to predict the critical load (P_{cr}) at a given lateral displacement as:

$$P_{cr} = \left(\frac{A_r}{A_b}\right) P_{cro} \tag{2.9}$$

where A_r is the reduced area corresponding to the overlapping area between the top and the bottom bearing end-end plate as illustrated in Fig.2.4.

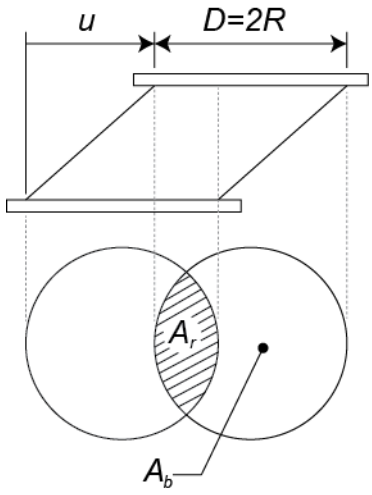

Figure 2.4. Illustration for overlapping area on a laterally deformed circular bearing

From Eq. 2.9, it can be concluded that the predicted vertical load capacity is zero when the shear displacement is equal to the diameter of the bearing. Past experimental data (Weisman and Warn 2012; Sanchez et al. 2011) has shown the overlapping area method to be conservative at large lateral displacements. Despite the inaccuracy, the overlapping area method is used in this study as it is currently employed in practice.

2.4 Effect of the vertical component of earthquake ground shaking on structural and non-structural systems

Historically for design purposes the demands due to the vertical component of ground shaking was assumed to be 2/3 of the horizontal demands (IBC 2000). However, inspection of recorded near-field ground motion (Loma Prieta 1989, Northridge 1994) has shown the vertical-horizontal spectral ratio can exceed 2/3 with values ranging as high as 1.7 for short periods (Bozorgnia et al. 1995). Due to the alignment of the structure period with the dominant vertical spectrum of earthquake excitations, researchers have recognized the damage potential of the vertical component of earthquake ground motion to fixed-base structures.

2.4.1 Damage due to vertical component in fixed-base structures

Reconnaissance following past earthquakes (Loma Prieta 1989, Northridge 1994, Kobe 1995) has revealed damage to structural and nonstructural systems in buildings that was attributed to large demands from the vertical component of ground shaking (Papazoglou and Elnashai 1996). Observed structural damage has included the collapse of columns due to abrupt increase in axial load demand, or shear compression failure as observed in the 3-story parking structure at the California State University during the Northridge earthquake (Hilmy and Masek 1994). The parking structure was constructed with a ductile perimeter moment resisting frame to sustain lateral earthquake loads while the internal columns support gravity loads. During the earthquake, some of the interior columns suffered total collapse due to compression failure while columns in the perimeter frame did not exhibit signs of distress beyond those attributed to the horizontal shaking demands. The stark difference between the performance of the interior and perimeter columns suggests failure of the interior columns can be attributed to large demands from the vertical component of ground shaking.

Damage to floor slabs has also been observed following the Northridge earthquake, for example, the collapse of waffle slabs in the upper two floors of the Bullocks store in Fashion Island Mall (Hall 1995). In this particular structure, the majority of the columns supporting these slabs showed only minor damage suggesting the collapse of the slabs could be attributed to large vertical stiffness demands due to the vertical component of ground shaking. Another example of damage to floor slabs was observed in the Northridge Fashion Centre north-west parking structure. The simply supported double-tee floors of this building experienced severe vertical motions leading to the development of shear cracks and ultimately total collapse of the floor system (Goltz, ed. 1994). The failure was attributed to the vertical component of excitation as the floor system was independent of the lateral load resisting system.

2.4.2 Damage due to vertical component in isolated structures

There has been no damage observed in base isolated buildings that has been attributed to the vertical component of ground shaking. However, damage has been observed during full-scale shake table tests of isolated building (Sato et al. 2011 and Ryan et al. 2012) at E-Defense, the largest capacity facility in the world with three dimensional shaking and interaction effects.

Furthermore, an elastomeric bearing with high shape factor (S = 30) has its vertical frequencies in a same magnitude range compared to that of fixed-base structure (Appendix H). Therefore, damage observed in fixed-base buildings is likely to happen for buildings isolated on high shape factor bearings.

Ryan et al. (2012) performed a full-scale testing of a 5-story steel moment resisting frame building isolated on triple friction pendulum and cross linear lead rubber bearings. The building was subjected to two-dimensional excitations (horizontal) and three-dimensional excitations (horizontal and vertical). Ryan reported a content disruption and ceiling tiles falling in the fifth floor of the buildings which was explained as an amplification of floor vertical accelerations in fifth floor to ground motion input (4g at 5^{th} floor compared to 1.3g PGA). The vertical floor acceleration was further amplified when the building was subjected to three-dimensional excitations, which could be explained by the rotation of the shaking table because of the couple between horizontal and vertical excitations.

2.5 Past effort to achieve three-dimensional isolation:

Researchers have recognized the potential adverse effect of the vertical component of ground motion for critical structures (e.g., hospitals, nuclear, among others) isolated on traditional high shape factor elastomeric and sliding bearings. Tajirian et al. (1990) proposed using low shape factor elastomeric bearings (i.e., $S = 2.3$) to achieve flexibility in both horizontal and vertical direction for three-dimensional isolation of nuclear structures. In their research, Tajirian performed dynamic tests on six quarter size prototypes of low shape factor elastomeric bearings. The results of the analysis and design work suggested that low shape factor is feasible for low rise building like SAFR (Sodium Advanced Fast Reactor) as the rocking and overturning effect is lessened due to the low height-width ratio of the structure. However, system level testing and analysis were not performed to verify the low shape factor concept. Furthermore, one challenge with using low shape factor approach will be balancing the conflicting objectives of shifting the period, that requires sufficient mass, and ensuring bearing stability.

A three-dimensional isolation system composed of helical springs, the GERB vibration controlled system, was developed by Huffmann (1984) and originally implemented for the three-dimensional seismic protection of diesel and turbo generator. An experimental study performed

by Huffmann (1984) on a reduced scale 3-bay, 5-story structure showed a reduction of horizontal acceleration could be achieved with the GERB system compared to the structure in the fixed-base configuration. However, amplification of ground acceleration was observed in a residential building in California isolated with the GERB system shaken during the 1994 Northridge earthquake (Makris and Deoskar, 1996). The maximum recorded top floor acceleration was approximately 0.63g in comparison to the estimated peak ground acceleration of 0.5g suggesting the GERB system did not provide effective isolation and raised questions regarding the effectiveness of the GERB system.

Research for three-dimensional isolation has been actively pursued in Japan to protect nuclear power plants against severe earthquakes. Three-dimensional seismic isolation system has been proposed by Takahashi et al. (2008) using a combination of air springs, laminated rubber bearings, and dampers with rocking prevention mechanism. This system consists of high damping laminated bearing, which is responsible for isolation in horizontal direction, sitting on top of a steel frame supported by air springs providing vertical isolation. Dampers are used to further dissipate energy in the system as well as limiting rocking from vertical motion. Two oil dampers are connected by cross-coupled pipes so that oil can move between dampers. When both dampers move up simultaneously, the pipes move up together. However when rocking occurs (one damper moves up, the other moves down), the cross-coupled pipes will restrict this movement and suppress rocking. Kageyama et al. (2002, 2004) proposed a concept of three-dimensional isolation air springs. This device supports and isolates a superstructure by compressed air springs, which consist of rubber layers between the inner and outer cylinders reinforcing polyester fabric and wire cables. The gap between inner and outer cylinders allows the device to move in both horizontal and vertical directions providing a reported fundamental period exceeding 3 seconds in both horizontal and vertical directions. However, these systems are unlikely to be implemented in United States due to their complexity, cost and unproven reliability.

2.6 Seismic Fragility Data of Nonstructural System

Fragility analysis has been used in recent years as a main tool to assess seismic vulnerability of structural and nonstructural systems. Seismic fragility has been defined as the conditional probability of failure of a system for a given intensity of a ground motion. Failure

occurs when the structure does not satisfy the requirements of a prescribed performance level. If the intensity of the ground motion is expressed as a single variable (e.g., the peak ground acceleration or the maximum earthquake spectral acceleration at short periods), the conditional probability of failure expressed as a function of the ground motion intensity is called a seismic fragility curve (Sasani and Der Kiureghian, 2001).

Non-structural damage in building structures has been widely observed and reported in past earthquakes such as cracking and collapse of masonry panel (Braga et al. 2009) or failure of a hospital's electrical supply (Reitherman et al. 1994). Although the vulnerability of nonstructural systems is well known, there is limited seismic fragility data for these systems, especially test data that includes the vertical component of excitation. One study by Badillo et al. (2006) performed seismic fragility testing of suspended ceiling systems that included both horizontal and vertical excitation. To facilitate testing of the suspended ceiling systems, a 16 ft by 16 ft steel frame was constructed and attached to an earthquake simulator platform. The ceiling systems consisted of 64 titles installed in a grid hung by suspension wires from the top of the test frame. Accelerometers and displacement transducers located at the center of the shake table were used to record the motion of the simulator platform, the test frame and the ceiling support grid, in each ceiling system. In the report by Badillo et al., the excitation at the top of the simulator platform is referred to as the floor acceleration. The test program consisted of subjecting the frame and ceiling system to synthetic horizontal and vertical excitations. The synthetic ground motion was generated from design spectra where the vertical design spectrum was obtained by scaling the amplitude of the horizontal spectrum by 2/3. A series of simulations in which the amplitude of both the horizontal and vertical excitations were simultaneously increased were performed for each type of ceiling system. The amplitude of the horizontal excitation was increased such that the target short period spectral acceleration (0.2s) ranged from 0.25g to 2.5g.

For the seismic fragility testing, four damage limit states were defined to characterize the seismic performance of the ceiling systems as listed in Table 1. Limit state 1 is considered minor damage with 1% loss of tiles. This level of damage is assumed to have little to no impact on the post event functionality of the building. Limit state 2 is defined as 10% loss of tiles. This limit state represents a level in which there would be a small loss of functionality. Limit state 3 is

defined as 33% loss of tiles and is associated with the level of life-safety. Finally, limit state 4 (grid failure) is defined by observation of localized grid failures leading to tiles lost or grid-assembly failures and is independent of the first three limit states.

Table 2.1 Limit State description from Badillo et al. 2006

Limit State	Description	Description
1	Minor	Loss of 1% of tiles from the suspension grid.
2	Moderate	Loss of 10% of tiles from the suspension grid.
3	Major	Loss of 33% of tiles from the suspension grid.
4	Grid Failure	Failure of part or the entire suspension grid.

A total of six set-ups were tested using different combinations of: (1) undersized tiles; (2) undersized tiles with retainer clips; (3) undersized tiles with recycled grid components; (4) normal sized tiles; (5) normal sized tiles with retainer clips and (6) normal sized tiles without compression post. Each set-up was tested repeatedly with the protocol described above. Trials are defined as the number of times one set-up was tested thoroughly and there were 6 trials for normal sized tiles set-up. Peak floor acceleration and spectral acceleration at periods of 0.2, 0.5, 1.0, 1.5 and 2.0 seconds were used as two demand parameters to construct fragility curves. For each set-up the following steps were taken to construct fragility curves:

1. Specify excitation amplitude
2. Perform test
3. Record simulator motion and identify peak acceleration
4. Count the number of fallen tiles following each simulation
5. Calculate the percent of fallen tile failure using the total number of tiles
6. Calculate the probability P_f of reaching or exceeding the limit state as: $P_f = N_f / N$ where N_f is the number of trials where the limit state was exceeded and N is the total number of trials
7. Determine parameters of the lognormal distribution function
8. Plot fragility curve: the probability of exceeding a limit state versus the corresponding peak floor acceleration

The fragility data for normal tile size configuration was adapted for this study. Due to the 2/3 vertical-horizontal relationship, data had to be interpolated for use in this study. The procedure for interpolating data from Badillo et al. (2006) is described in Chapter 3.

2.7 Summary and Research Justification

- Damage to structural elements in fixed-base structures has been observed and attributed to the vertical component of ground shaking.

- Isolation systems composed of high shape factor bearings ($15<S<25$) have low vertical periods (0.03s-0.15s) that aligns with the region of the vertical spectrum where there is significant amplification.

- Vertical acceleration demands ranging from 1.3g to 4g were observed in the upper stories of a full-scale five-story steel building during recent earthquake simulation tests that included the vertical component of excitation. Damage to suspended ceiling systems was also observed attributed to large vertical acceleration demands.

- Past efforts to achieve three-dimensional isolation are either not viable (low shape factor) or costly and have unproven reliability (Japanese systems).

- There is a lack of a systematic understanding of how the vertical properties of the isolation system affect vertical demands and the likelihood of damage to structural and nonstructural components.

Chapter 3

Research approach

3.1 General

This chapter provides details of the prototype structures, analytical models and protective systems considered in this study. Twenty sets of ground motions used for response history analysis are briefly described. Finally, information to formulate fragility curves used to estimate damage to suspended ceiling system is provided at the end of this chapter.

3.2 Methods

1. Develop analytical models of base isolated frames.
2. Perform parameter study on shape factor (S)
3. Evaluate performance of suspended ceiling system using fragility curves adopted from Badillo et al. 2006
4. Modify based isolated frames to mitigate damage as follow:
    - Added vertical damping
    - Vertical distributed flexibility
5. Evaluate mitigation schemes

Figure 3.1 illustrates three different analytical model configurations used in this study, namely: (1) structure with conventional base isolation, (2) structure with conventional base isolation and vertical supplemental dampers, and (3) structure with conventional base isolation and column isolators.

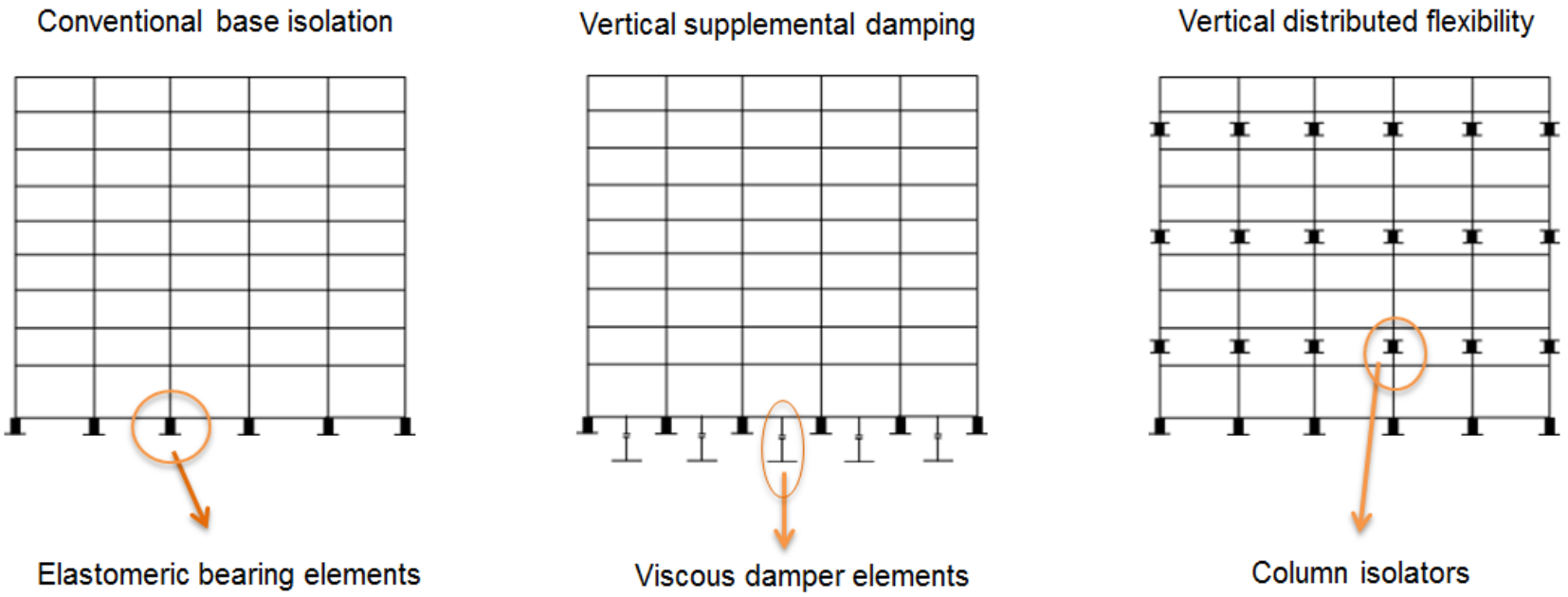

Figure 3.1. System configurations

3.3 Prototype superstructure

The three-story and nine-story pre-Northridge steel moment frames developed by Gupta and Krawinkler (1999) for the SAC (a joint venture of the *S*tructural Engineers Association of California, *A*pplied Technology Council and *C*alifornia Universities for Research in Earthquake Engineering) steel project were selected as the prototype super-structural systems for the models used in this study. These structures are office buildings located in Los Angeles, California, designed according to the 1994 UBC building code. Schematics for the floor plans and elevations of the three-story and nine-story buildings are shown in Fig. 3.2. Both structures consist of perimeter moment resisting frames to resist lateral earthquake loads and interior gravity frames. For this study, only the north-south perimeter moment frames were considered for the two dimensional analytical model. Member section sizes for the perimeter moment frames of the three-story and nine-story frames are summarized in Tables 3.1 and 3.2. In Fig 3.2, "L" indicates lateral force resisting frame and "G" indicates gravity frame. Further details pertaining to the design of the moment frames can be found from Gupta and Krawinkler (1999) report.

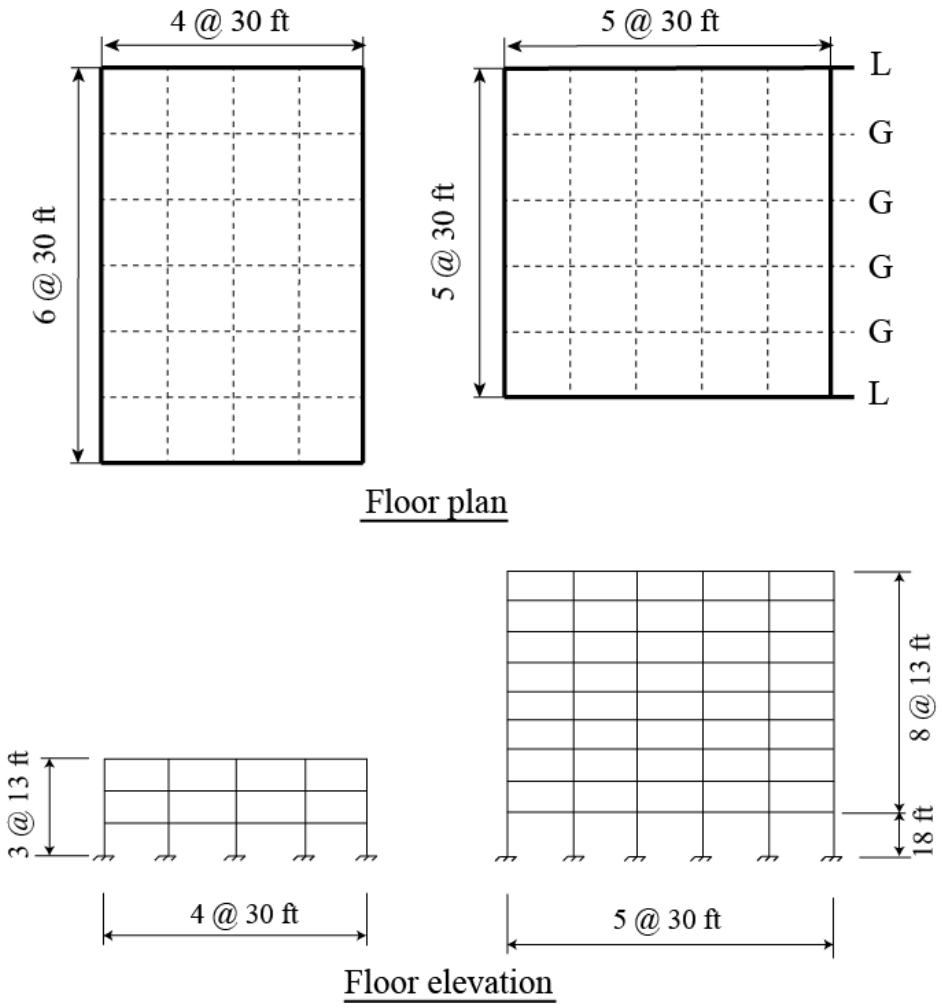

Figure 3.2. Floor plan and elevation for three and nine-story office buildings

The member sections of the north-south moment resisting frame are provided in the table 3.1 and table 3.2. Also provided in these tables are the floor masses for each story. The floor masses were obtained directly from Gupta and Krawinkler report (1999). Details of loads provided by Gupta and Krawinkler (1999) are presented in Appendix A.

Table 3.1 Three-story frame details

Story	Columns		Girder	Mass (kips-sec^2/ft)
	Interior	Exterior		
1	W14x311	W14x257	W33x118	65.53
2	W14x311	W14x257	W30x116	65.53
3	W14x311	W14x257	W24x68	70.90

Table 3.2 Nine-story frame details

Story	Columns		Girder	Mass (kips-sec^2/ft)
	Interior	Exterior		
1	W14x500	W14x370	W36x160	69.04
2	W14x500	W14x370	W36x160	67.86
3	W14x455	W14x370	W36x135	67.86
4	W14x455	W14x370	W36x135	67.86
5	W14x370	W14x283	W36x135	67.86
6	W14x370	W14x283	W36x135	67.86
7	W14x283	W14x257	W30x99	67.86
8	W14x283	W14x257	W27x84	67.86
9	W14x257	W14x233	W24x68	73.10

3.4 Analytical model

In this research, only north-south perimeter moment resisting frames ("L" as shown in Fig. 3.2) were considered for the analytical study. The gravity frames have negligible effect on seismic response and the design of north-south and east-west moment resisting frames is similar. Two-dimensional models were used instead of three-dimensional models to eliminate difficulty with modeling floor system. Models were developed using the OpenSees (Open System for Earthquake Engineering Simulation 2009) software that is developed and provided by the Pacific Earthquake Engineering Research (PEER) Center (http://opensees.berkeley.edu).

3.4.1 Superstructure system

The base isolation system was proportioned using the yield strength of the perimeter frames obtained from push-over analysis (Gupta and Krawinkler 1999) so that the base isolated super-structure would remain elastic or nearly elastic during a design basis event. For this reason, the superstructure elements were modeled using beam-column elements with linear elastic material properties. Each element was assigned the appropriate member's cross-sectional area and moment of inertia according to the prototype frames (see Tables 3.1 and 3.2). The modulus of elasticity and Poisson's ratio for each member were specified to be 29,000 ksi and 0.3, respectively. Finally, beam-column connections were modeled rigidly.

3.4.2 Mass and Loadings

In these models, mass is lumped at nodes at the intersections of the beams and columns. In order to represent a three-dimensional building using a two-dimensional model the mass had

to be separated into vertical and horizontal components and distributed to the nodes of the perimeter frame accordingly. The two perimeter moment frames (see Fig. 3.2) provide the lateral force resistance for the entire building. A half of the horizontal floor mass is assumed to be carried by the moment frame through diaphragm action. To represent the horizontal mass in the 2D model, one-half (5m) of the floor mass was lumped at corresponding nodes of the 2D model as illustrated in Fig. 3.3.

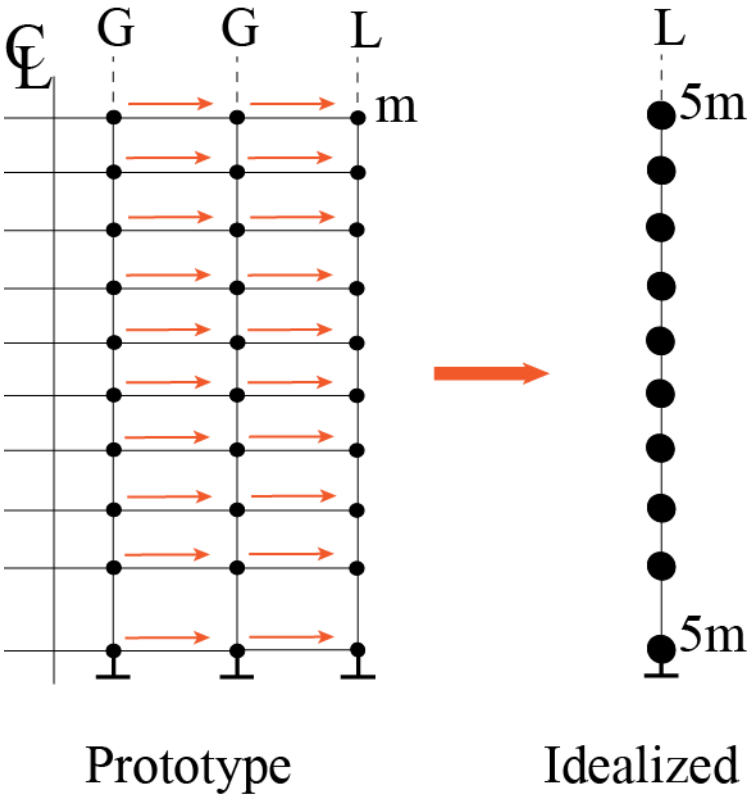

Figure 3.3. Horizontal distribution of mass for 2-dimensional moment resisting frame

The vertical load carried by the perimeter frame, however, is based on tributary floor area. The vertical mass carried by the perimeter frame is therefore the tributary mass "m" and the vertical mass carried by gravity frames is “2m”. Since half of the building is being modeled as 2D frame, the vertical load carried by the gravity frames therefore must be included in the 2D model. To account for gravity loads transmitted to isolation system not by way of the moment frame, the vertical mass carried by the gravity frames was lumped at the base of the 2D model above the plane of isolation as illustrated in Fig. 3.4.

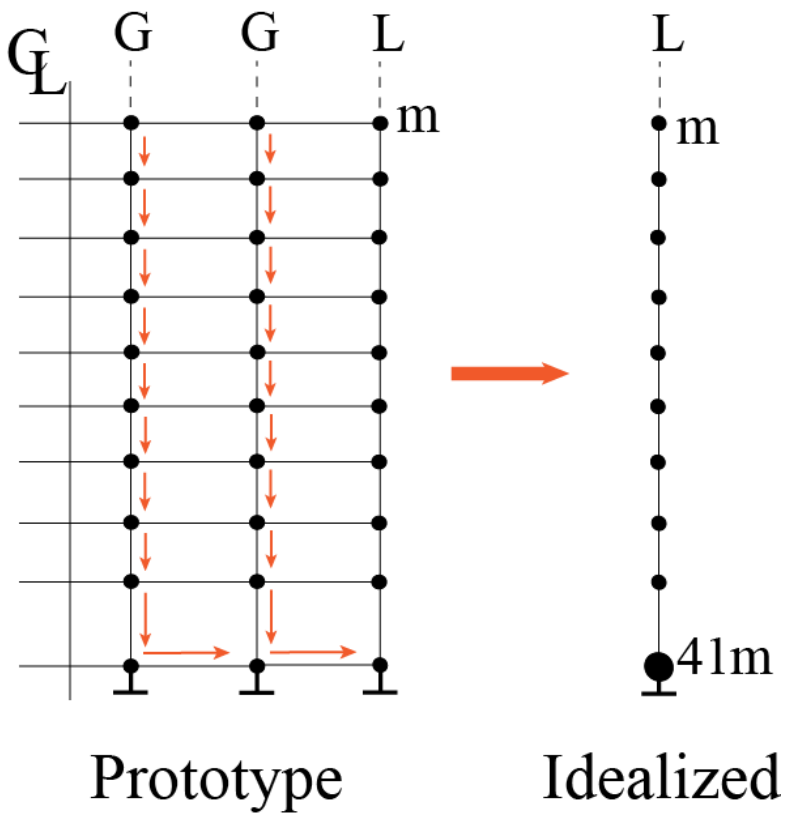

Figure 3.4. Vertical distribution of mass for 2-dimensional moment resisting frame

3.4.3 Elastomeric bearings

The base isolators were modeled using the *Elastomeric Bearing* element in OpenSees. This element uses a coupled plasticity model (Huang et al. 2000) to represent the lateral force-deformation behavior of the bearing that is characterized using the bilinear force-deformation relationship shown in Fig. 3.5. The bi-linear characterization shown in Fig. 3.5 is defined by the following parameters: Q_d the zero-displacement force-intercept; K_d the second-slope stiffness; K_u the elastic stiffness; K_{eff} the effective (or secant) stiffness and the energy dissipated per cycle

(EDC). Further details needed to model the elastomeric bearings for three and nine-story frames are provided in Appendix D.

The vertical force-deformation behavior was also modeled having bi-linear relationship (Fig 3.5) to account for inherent vertical damping property of rubber. Fig 3.6 illustrates the first system configuration considered in this research: 3- and 9-story frame with conventional base isolation.

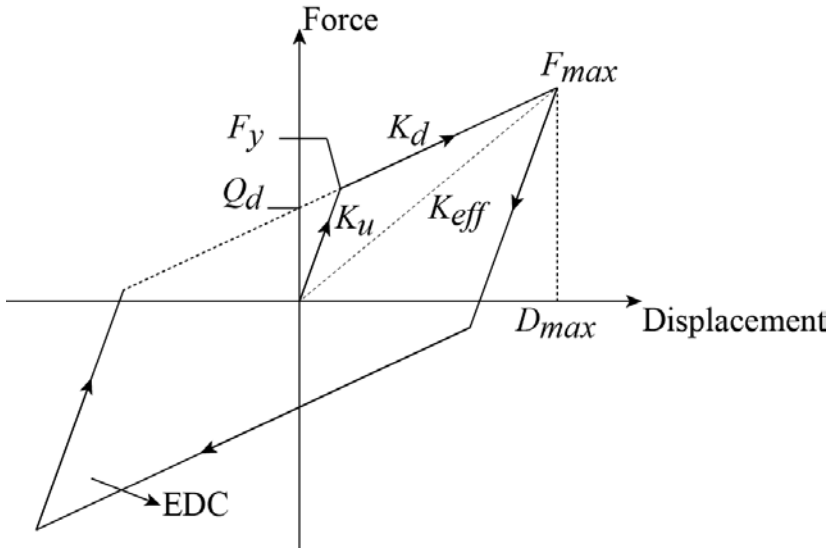

Figure 3.5. Bilinear force-deformation characterization for elastomeric bearing

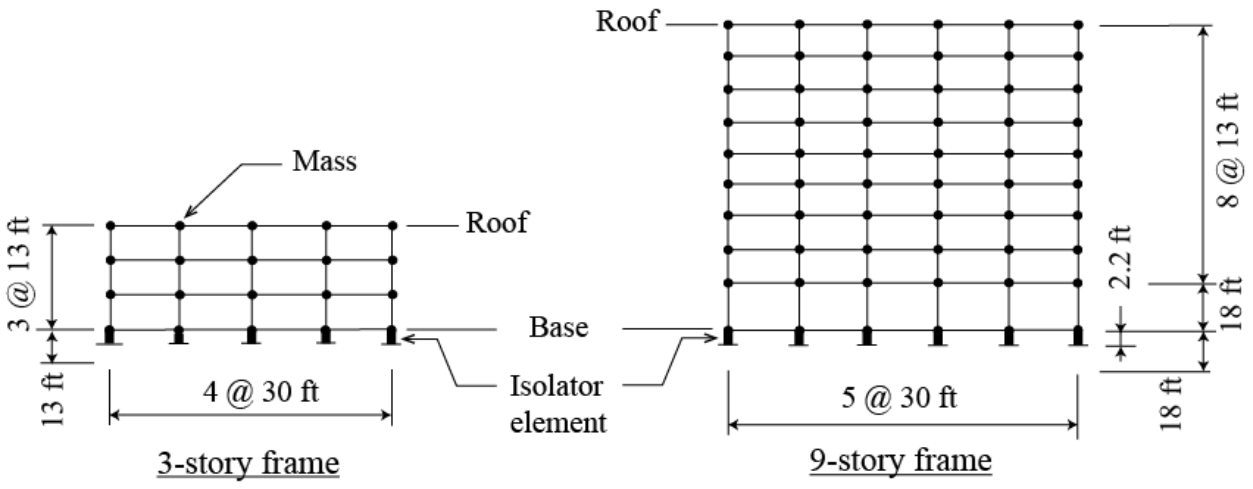

Figure 3.6. Illustration of 3- and 9-story frame with conventional base isolation

3.4.4 Dampers

As described in section 3.2, the benefit of viscous fluid dampers for mitigating damage to nonstructural systems in the upper stories of the base-isolated superstructure is explored as part of this study. The viscous dampers were modeled at the plane of isolation and oriented in the vertical direction as illustrated in Fig. 3.7. The dampers are modeled using *Truss element* in OpenSees (2009). Each truss element was assigned viscous-elastic material to represent the rate dependent force-deformation behavior of viscous-fluid dampers. The damper elements were assumed to be linear-viscous with a velocity exponent equal to 1 and a damping coefficient *c*. The damping force (F_D) is expressed as follows: $F_D = c\dot{u}$. The length of the damper elements was specified to be equal to the height of the first story of each frame to minimize rotation from the vertical orientation due to lateral displacement of the isolation system.

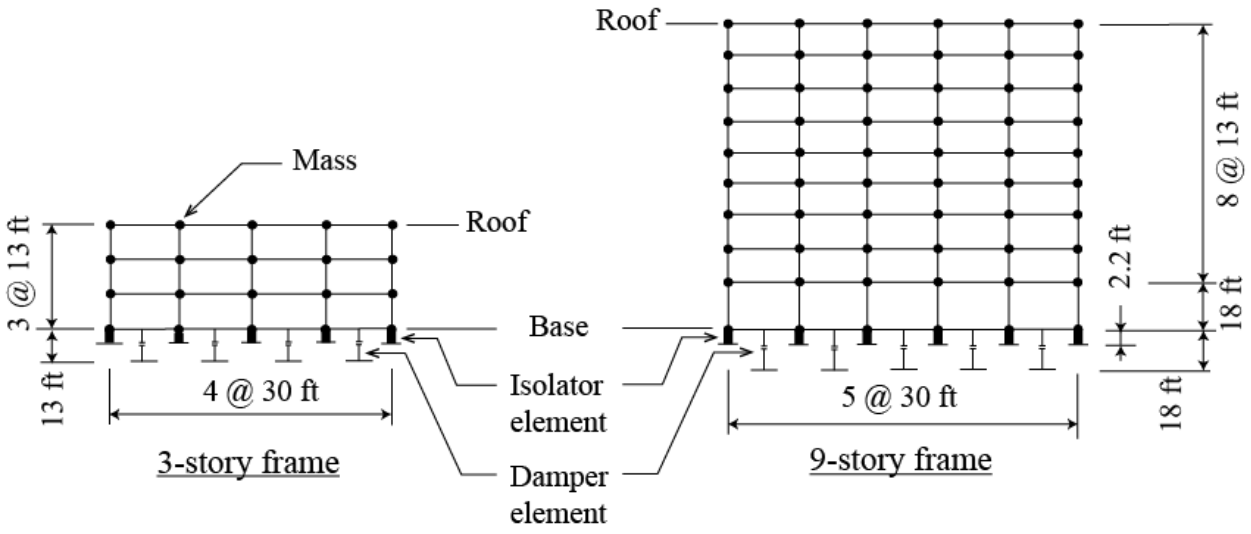

Figure 3.7. Illustration of 3- and 9-story frame with conventional base isolation and supplemental viscous dampers

3.4.5 Column isolators

As described in section 3.2, a vertically distributed flexibility scheme is considered in this study to minimize or eliminate damage to nonstructural systems due to the vertical component of ground shaking. Vertical flexibility in the superstructure is achieved by introducing bearings in the column line of the upper levels of the superstructure as illustrated in Fig. 3.8. Zero-length elements (OpenSees 2009) were used to model column bearings. The zero-length element is

connected to two nodes at the same location. These nodes are constrained laterally (translate together) and in rotation but are allowed to displace relative to each other in the vertical direction. The vertical force-deformation behavior was modeled using a bilinear material to account for hysteretic behavior of multi-layer rubber bearings in compression. The positions of column bearing elements are chosen between columns below story 2 for a 3-story model (Fig. 3.8) and between columns below story 2, 5 and 8 for a 9-story model.

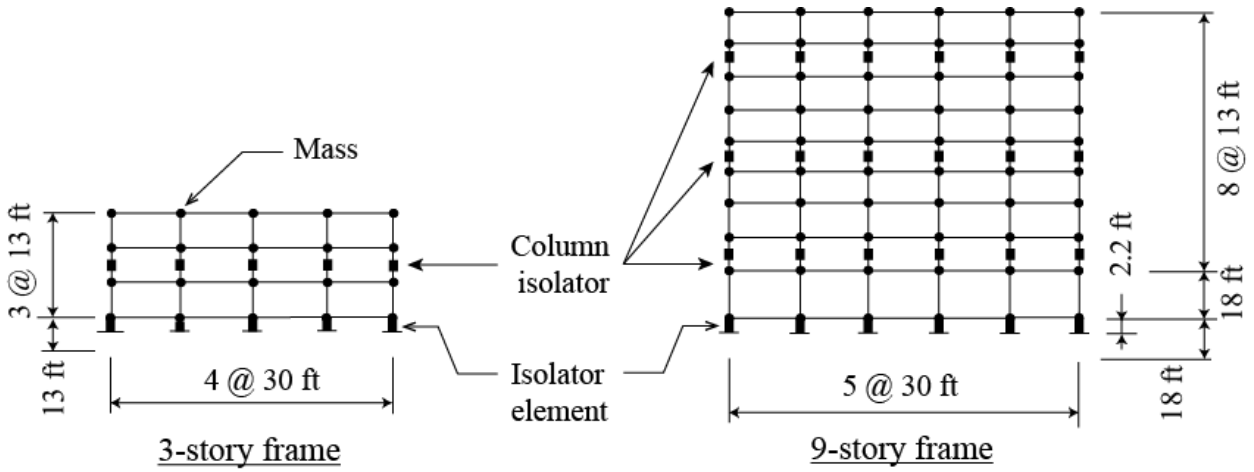

Figure 3.8. Illustration of 3- and 9-story frame with conventional base isolation and column isolators

Figure 3.9 is a sketch to illustrate one potential column isolator scheme. The column isolator shown in Fig. 3.9 is constructed of rubber layers bonded to steel plates simulates a traditional laminated rubber bearing. A steel dowel connected to the top end plate would resist lateral movement by bending against the bottom end plate but allow vertical movement through a gap as shown in Fig. 3.9.

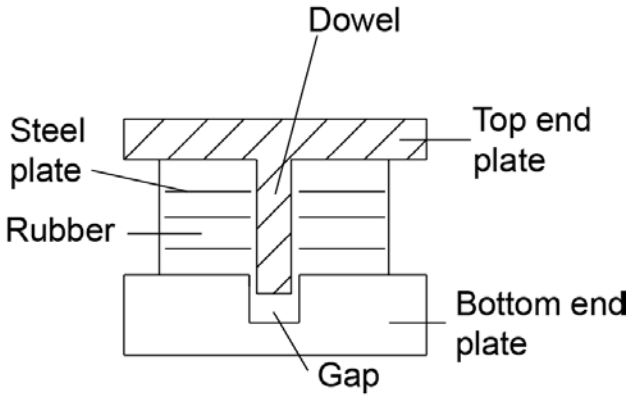

Figure 3.9. Illustration of column isolators

3.5 Earthquake ground motions

Recorded earthquake ground motions obtained from historical earthquake events were collected and used to facilitate response history analysis of the analytical models. A set contains 2 horizontal and 1 vertical component ground motions which are obtained from the Pacific Earthquake Engineering Research ground motion database (PEER 2011). Twenty sets of earthquake ground motions were organized into a bin. Summary information for this bin is presented in Table 3.3. Details of the individual ground motions contained in Bin 1 can be found in Appendix B. Individual and average elastic, 5% of critical damping, acceleration response spectra generated from the horizontal and vertical components of ground motions contained in Bin 1 are shown in Fig. 3.10. The average spectra presented in Fig. 3.10 was considered design spectra and used to design the protective systems including the base isolation systems for the three- and nine-story frames. A design 5 percent damped spectral acceleration parameter at 1s period is 0.84g from Fig. 3.10.

Table 3.3 Summary of ground motion bins

Bin	Number of ground motions/sets	Site class (USGS classification)	Distance to rupture surface (km)	Moment Magnitude
1	30/10	A & B	0.96 - 8.88	6.7 – 7.6

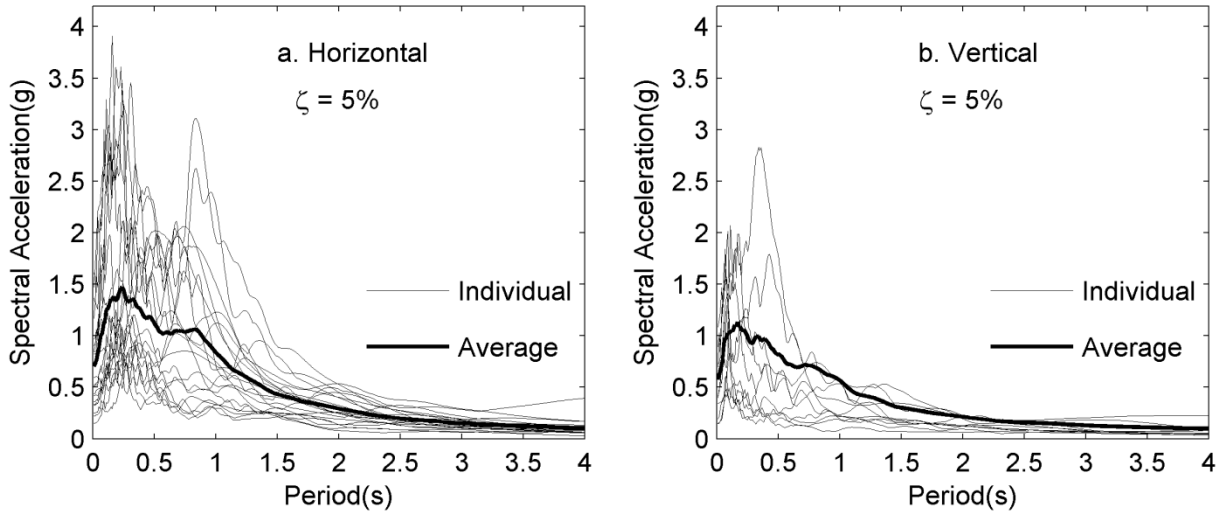

Figure 3.10. Elastic, 5% damping, earthquake response spectra for Bin 1: (a) horizontal spectra; (b) vertical spectra

3.6 Design of protective system

3.6.1 Base isolation

The base isolation system is designed so that the superstructure remains elastic under a design level event. A push-over analysis of the fixed-base three- and nine-story frames was performed to determine the elastic capacity of the frames (V_s). Results of the push-over analysis of the three- and nine-story frames are provided in Appendix C.

From the push-over analysis, the maximum base shear that the structure can sustain while remaining elastic (V_s) was determined. The following equation derived from Eq. 17.5-1 and Eq. 17.5-8 (ASCE 2010) is used to calculate the design period (T_D) for the superstructure to remain elastic:

$$T_D \geq \frac{S_{D1}W}{R_I B_D V_s} \tag{3.1}$$

where S_{D1} is a design 5 percent damped spectral acceleration parameter at 1s period in units of g (acceleration due to gravity), B_D is a numerical coefficient related to the effective damping of the isolation system (B_D = 1.2 for 10% damping), R_I is the numerical coefficient related to the type of seismic force-resisting system above the isolation system (R_I = 1.5 for an isolated moment resisting frame) and W is the weight of the entire structure (superstructure and seismic isolation system).

The designed horizontal displacement of the isolation (ASCE 2010) is calculated as:

$$D_D = \frac{gS_{D1}T_D}{4\pi^2 B_D} \tag{3.2}$$

where g is the acceleration due to gravity calculated in units of in/s^2. The effective horizontal stiffness of the seismic isolation system (AASHTO 2010) is calculated as:

$$K_{eff} = \left(\frac{2\pi}{T_D}\right)^2 \times m \tag{3.3}$$

where m is the mass of the whole structure. The effective stiffness of the entire isolation system is then distributed to each isolation bearings in the ratio of 1:2 for exterior and interior columns

so that the static pressure in every bearing is similar. Table 3.4 presents details of the designed isolation systems for the 3- and 9-story frame. Further details for individual elastomeric bearings are provided in Appendix D.

Table 3.4 Details of isolation system properties

Frame	Design period (sec.)	Effective stiffness (kips/in)	Design displacement (in)
3	2	99	13.7
9	3.5	89	24

3.6.2 Column isolators

There is no codified procedure to proportion the column isolator. Instead, the column isolators were proportioned so that the critical load capacity of the bearings satisfied the AASHTO (2010) service stability requirement:

$$\frac{P_{cro}}{P_D + P_L} \geq 3 \tag{3.4}$$

where P_{cro} is the critical load capacity of the bearing in the laterally un-deformed configuration (Eq. 2.7). It is assumed that the height of column bearings are 4 in and the static pressures in these bearings range from 0.5-0.75 ksi. A summary of the column bearing design is presented in Table 3.5 including the resulting vertical stiffness calculated according to Eq. 2.2 presented in Chapter 2. Details for individual column isolators are provided in Appendix G.

Table 3.5 Summary of column isolators' properties

Frame	Gravity loads (kips)		P_{cro} (kips)		P_{cro} / Gravity load		Vertical stiffness (kips/in)	
	Exterior	Interior	Exterior	Interior	Exterior	Interior	Exterior	Interior
3	56	112	193	386	3.45	3.45	360	509
9-floor 2	253	506	809	1620	3.2	3.2	1304	1844
9-floor 5	155	309	475	948	3.07	3.07	669	944
9-floor 8	56	112	193	386	3.45	3.45	360	509

3.6.3 Viscous fluid damper

To calculate damping coefficient for the supplemental viscous fluid dampers, base isolation system and dampers are treated as linear, single degree-of-freedom (SDOF) system where the mass of the SDOF system is that of the superstructure (Fig. 3.11). The viscous damping coefficient (Chopra 2007) is calculated for the specific damping ratio using:

$$c = 2\xi\sqrt{km} \tag{3.5}$$

where c (kips-sec/in) is the damping coefficient, k (kips/in) is the vertical stiffness of the base isolation system and m is the mass of the super structure.

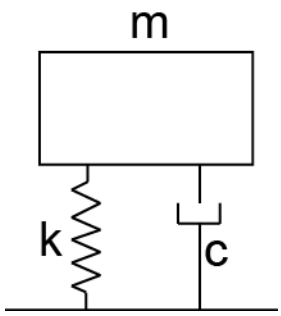

Figure 3.11. Illustrator for base isolation and viscous damper as single degree of freedom system

The damping coefficient is then divided evenly among the number of dampers assuming a parallel relationship. Values of damping coefficient for 3- and 9-story frame corresponding to 10% and 20% damping ratio are provided in Appendix E.

3.7 Parametric study

As described in Chapter 2 (see Eq. 2.6) the vertical stiffness of an elastomeric bearing is proportional to the horizontal stiffness by square of the shape factor. A parametric study was conducted to investigate the influence of the shape factor (i.e., vertical stiffness) of the isolation system on vertical acceleration demands in the upper stories of the seismic isolated building and fragility of the suspended ceiling systems. For the three-story and nine-story frames the vertical stiffness of the individual isolators was varied corresponding to shape factors ranging from 1 to 30.

In addition to varying the shape factor (i.e., vertical stiffness) the damping ratios for the supplemental viscous fluid dampers (as described in section 3.2) were varied between 0 and 20% of critical to investigate the influence of vertical supplemental viscous damping on vertical acceleration demands in the upper stories of the super-structure and fragility of suspended ceiling systems.

3.8 Formulation of fragility curves

Fragility data from Badillo et al. (2006) was adapted for this study to evaluate the effectiveness of the mitigation strategies described in section 3.2. From the results of tests conducted by Badillo et al. (2006), the performance of the suspended ceiling system is sensitive to the type of seismic input. More specifically, higher degrees of damage were observed when ceiling system was subjected to simultaneous horizontal and vertical excitations by comparison to only horizontal or vertical excitation. However, the tests performed by Badillo used synthetic ground motions that were generated from vertical and horizontal spectra related by the traditional 2/3 ratio. For a base isolated structure, the horizontal acceleration demands are expected to be much lower than the vertical, requiring the data presented in Badillo et al. (2006) to be interpolated for use in this study. Using data provided by Badillo et al (2006), fragility curves for peak vertical floor acceleration corresponding to a specified horizontal acceleration demand were developed. A step-by-step description of the process to construct the fragility curve for the minor damage state is as follows:

- Assemble data from Badillo tests as shown in Table 3.6 for the probability of exceeding minor damage of ceiling system;
- Interpolate data in Table 3.6 to calculate probability of exceeding minor damage for each vertical acceleration demand with a specific horizontal acceleration demand; achieve Table 3.7. A value of 0.85g peak horizontal floor acceleration was chosen for purpose of illustration.
- Determine parameters of the lognormal distributions;
- Perform the Kolmogorov-Smirnov (K-S) test for 5% significance level to validate the log-normal distribution and optimize log-normal distribution parameters;
- Plot the fragility curve of the probability of exceeding a limit state versus the peak vertical floor acceleration. The sample fragility curve is shown in Fig 3.12.

Table 3.6 Badillo data for minor damage probability of failure

	Probability of failure (%)					
PVFA(g) / PHFA(g)	0	0.735	0.853	0.941	1.02	1.1
0	0	0	0	0	0	50
0.781	0	0				
0.969	0		50			
1.14	17			100	100	100
1.51	33			100	100	100
2	83			100	100	100

Table 3.7 Interpolated data for a specified peak horizontal floor acceleration

	Probability of failure (%)					
PVFA(g) / PHFA(g)	0	0.735	0.853	0.941	1.1	1.15
0.85	0	0	44	75	87	100

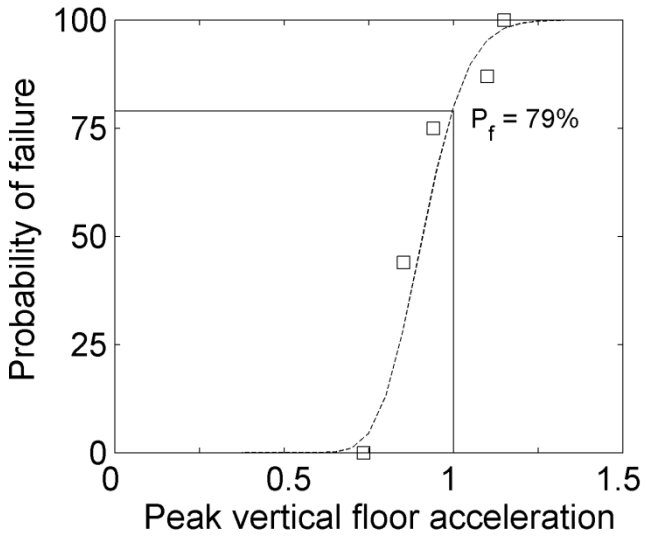

Figure 3.12. Sample fragility curve for peak vertical floor acceleration corresponding to peak floor horizontal acceleration 0.85g

From Fig. 3.12, the probability of having minor damage for a 1g vertical and 0.85g horizontal acceleration demand could be estimated as 79%. Fragility curves for peak vertical acceleration corresponding to peak horizontal acceleration equal to 0.85g and 0.05g are presented in Fig. 3.13 and 3.14. Curves are presented for the first three limit states that were defined in Table 2.1. Tables 3.8 and 3.9 present the values of the mean, standard deviation of the

log-normal distribution used to construct those fragility curves. Details to formulate Figs 3.13 and 3.14 as well as Tables 3.8 and 3.9 can be found in Appendix F.

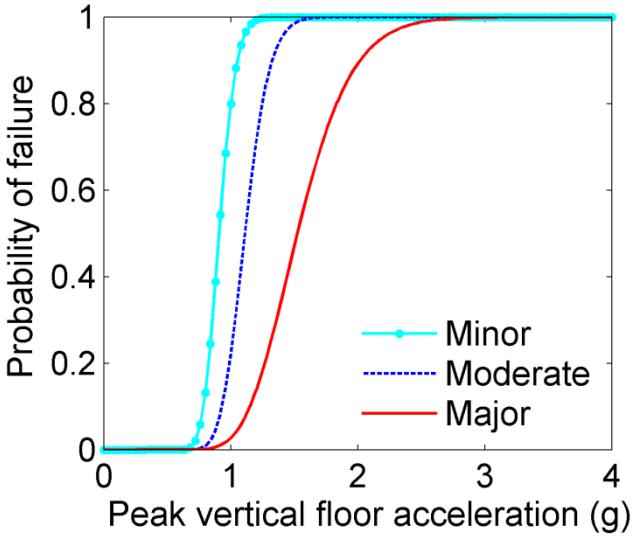

Figure 3.13. Fragility curve for peak floor vertical acceleration corresponding to peak floor horizontal acceleration 0.85g

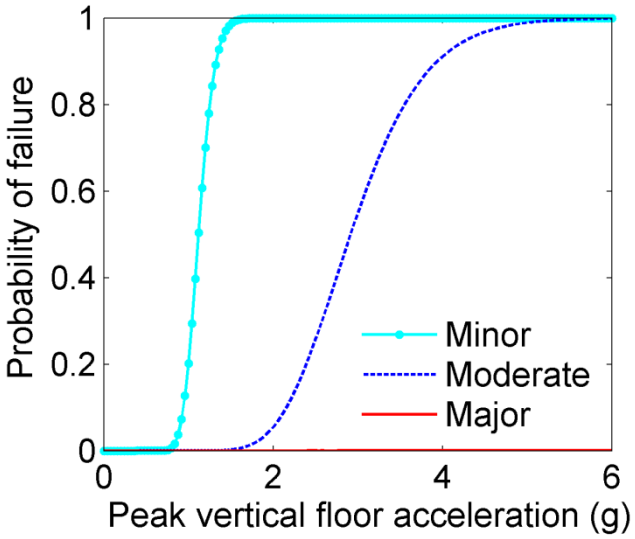

Figure 3.14. Fragility curve for peak floor vertical acceleration corresponding to peak floor horizontal acceleration 0.05g

In Fig. 3.14, the major line coincides with the axis meaning major damage is not going to happen until vertical acceleration demands exceed 6g.

Table 3.8 Log-normal parameters of fragility curve for PHA = 0.05g

	Mean (λ)	Standard Deviation (ξ)	Difference (D_n)
Minor	0.112	0.134	0.069
Moderate	1.07	0.235	0.03
Major	5	0.5	N/A

Table 3.9 Log-normal parameters of fragility curve for PHA = 0.85g

	Mean (λ)	Standard Deviation (ξ)	Difference (D_n)
Minor	-0.0956	0.114	0.151
Moderate	0.106	0.138	0.117
Major	0.422	0.219	0.075

3.9 Estimate probability of failure for ceiling systems

The probabilities of failure were calculated as the average values of twenty failure probabilities calculated from twenty analyses (P_f). This section illustrates how to use fragility curve to estimate probability of failure from vertical and horizontal acceleration demands from one analysis (P_i).

$$P_f = \frac{\sum_{i=1}^{n} P_i}{n} \tag{3.6}$$

As shown later in Chapter 4, peak floor horizontal acceleration ranges from 0.05g to 0.85g and by interpolating between the 0.05 and 0.85 fragility curves for a given vertical acceleration demand, a probability of failure for a single analysis can be calculated as shown in Fig. 3.15.

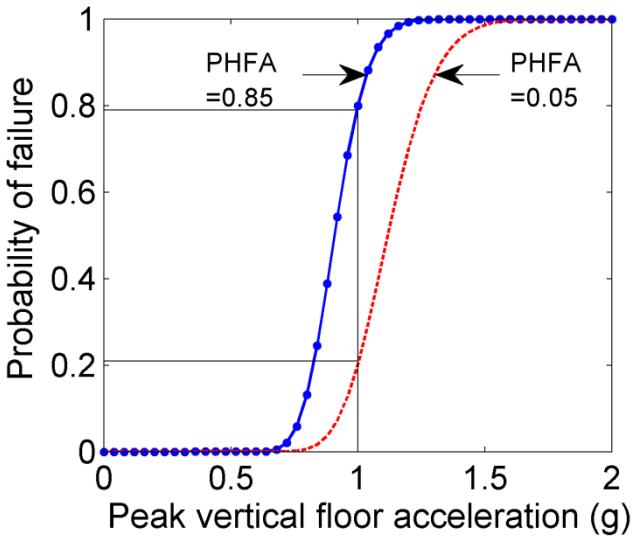

Figure 3.15. Illustration for estimate probability having minor damage

For instance, a probability of exceeding minor damage state in ceiling system is needed to be estimated knowing that the vertical and horizontal acceleration demands are 1g and 0.45g, respectively. Figure 3.15 shows that probability having minor damage as peak vertical acceleration = 1g and peak horizontal acceleration = 0.85g is 79%. Similarly, probability having minor damage as peak vertical acceleration = 1g and peak horizontal acceleration = 0.05g is 21%. An interpolation to estimate probability having minor damage as peak vertical acceleration = 1g and peak horizontal acceleration = 0.45g is (79+21)/2 = 50%.

Chapter 4

Analytical results

4.1 General

Results from the analytical studies are presented in this chapter. The primary metrics for assessing the performance of the various systems described in Chapter 3 are the vertical absolute acceleration demands in the superstructure and the probability that the suspended ceiling system exceeds a given limit state. These metrics are used to evaluate the three configurations, namely: base isolated frame; base isolation with supplemental damping and base isolation with vertically distributed column isolators. The vertical acceleration demands presented in this chapter are the average acceleration demands obtained from the results of twenty response history analyses of each individual model using the ground motion sets in bin 1. Finally, rough estimations of the probability of failure for ceiling systems were calculated using fragility data. It is important to note that the failure probabilities are a metric for comparison and not prediction.

4.2 Results from parametric study of the base isolated frames

A parametric study was conducted to investigate the influence of the vertical stiffness (i.e., shape factor) on acceleration demands and fragility of suspended ceilings in the upper levels of base isolated frames. Eighteen values of the shape factor were analyzed ranging from 1 to 30.

4.2.1 Horizontal acceleration demands

Average horizontal acceleration demands at all floor levels for 3-story and 9-story frames are plotted in Figs. 4.1 and 4.2 respectively. Horizontal accelerations demand presented in Figs. 4.1 and 4.2 are the average of twenty peaks horizontal acceleration demands at a particular floor in units of gravity (g). Figs. 4.1 and 4.2 show that the horizontal acceleration demands in both the 3- and 9-story frames are nearly constant for each different shape factor. This result was expected because changing shape factor only affects the vertical stiffness of the structures.

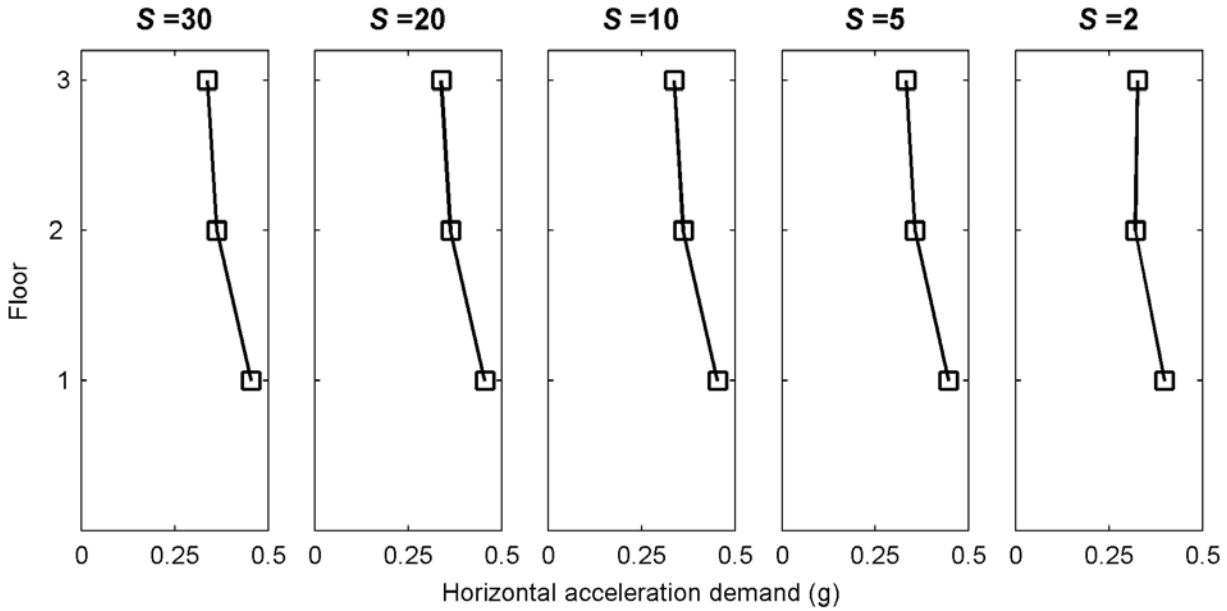

Figure 4.1. Average horizontal acceleration demands in 3-story frame at each floor level

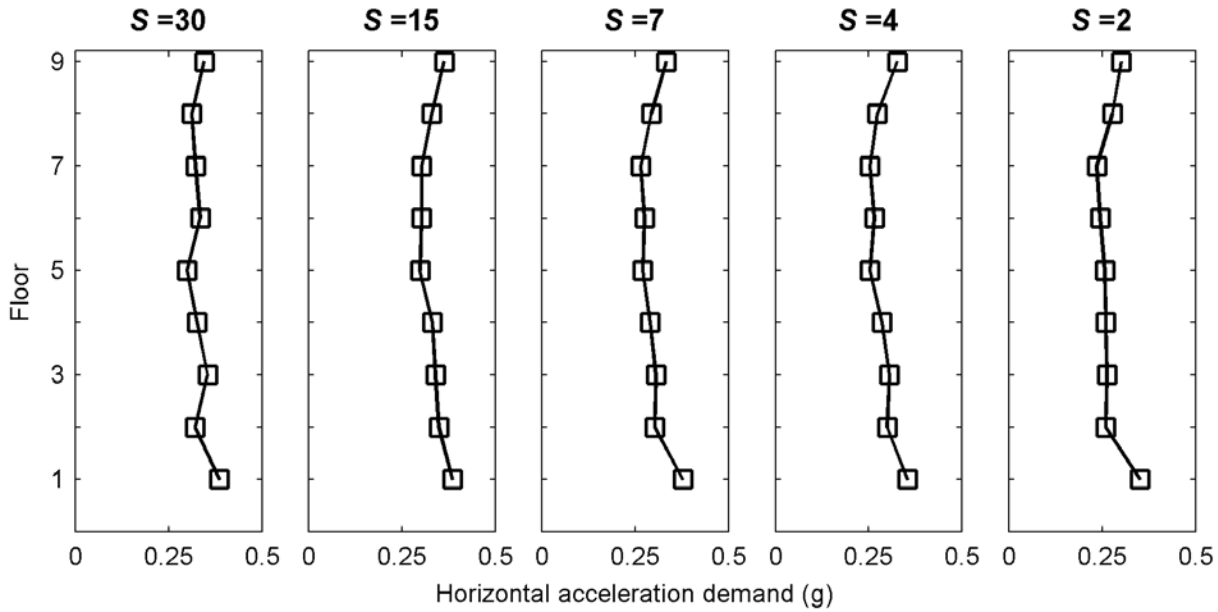

Figure 4.2. Average horizontal acceleration demands in 9-story frame at each floor level

Figures 4.3a and 4.3b present individual and average horizontal acceleration demands for 3- and 9-story frames at each floor level. The acceleration horizontal demands for the 3-story frame range from 0.074g - 0.823g and the acceleration horizontal demands for the 9-story frame range from 0.08g - 0.79g. Hence, fragility curve corresponding to 0.05g and 0.85g horizontal

acceleration demands were chosen as lower and upper boundary for estimating the probability of failure.

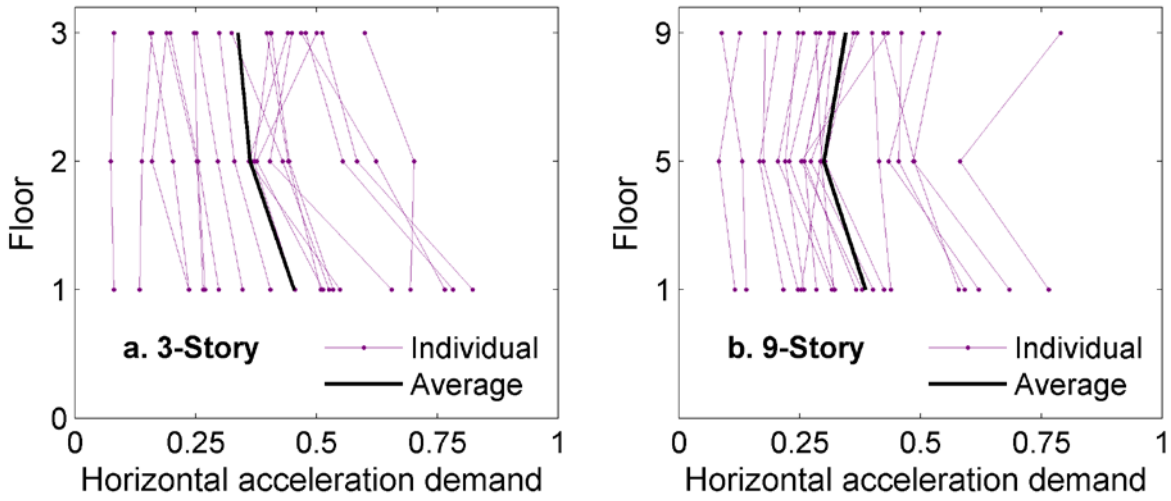

Figure 4.3. Individual and average peak horizontal acceleration demand at each floor level: (a) 3-story; (b) 9-story

4.2.2 Vertical acceleration demands

Figures 4.4a and 4.4b present the average peak vertical absolute acceleration demands at the base and roof of the 3- and 9-story frames, respectively. Peak vertical absolute accelerations demand presented in Figs. 4.4a and 4.4b are the average of twenty peak demands at a particular level normalized by gravitational acceleration (g). The acceleration demands at the base for the 3-story frame range from 0.43g - 0.79g. Average absolute acceleration demands at the roof of the 3-story frame are marginally larger with the range of 0.43g - 1.62g. The acceleration demands at the base for the 9-story frame range from 0.32g - 0.8g. There is a significant increase in acceleration demands at the roof level in the 9-story frame for high shape factor (e.g. S >15), with values as high as 4g for S=30. The results plotted in Fig. 4.4 show that, on average, there is amplification for all but the lowest shape factor (i.e., S = 1). Further, the results plotted in Fig. 4.4 shows, on average, that for shape factors greater than 5 the amplification at the roof is significantly larger than the base suggesting that the vertical accelerations are being amplified by the superstructure.

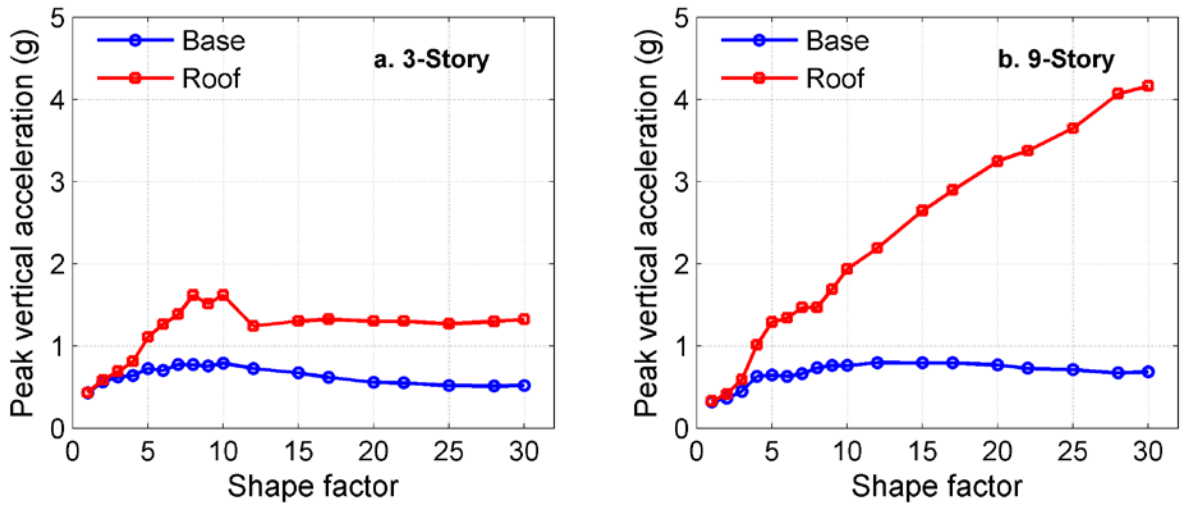

Figure 4.4. Average vertical acceleration demands versus shape factor: (a) 3-story and (b) 9-story

4.2.3 Fragility of suspended ceilings

Fragility curves generated from data presented in Badillo et al. (2006) were used with the vertical acceleration demands to estimate the probability of exceeding specific limit states. The probability information was then used to evaluate the performance of the isolated frame with different bearing shape factors. Average vertical acceleration demands at all floor levels for 3-story and 9-story frames are plotted in Figs. 4.5 and 4.7 respectively and the probability of exceeding three damage states for selected shape factors are plotted in Figs. 4.6 and 4.8. In Fig. 4.6, the first row plots presents the probability that damage from story 1 to 3 could exceed the minor state; the second row is the probability that damage exceed moderate state. Finally, the third row is the probability that damage exceed major state. The same interpretation could be applied for Fig. 4.8.

The probabilities of failure were calculated as the average values of twenty failure probabilities calculated from the vertical acceleration demands of twenty analyses. As described in Chapter 2, peak vertical acceleration recorded at the shake table was used to formulate the fragility curve for the ceiling system hence the peak vertical acceleration at floor 1 was used to assess damage for the ceiling system at story 1. This calculation was repeated for floors 2 to 9.

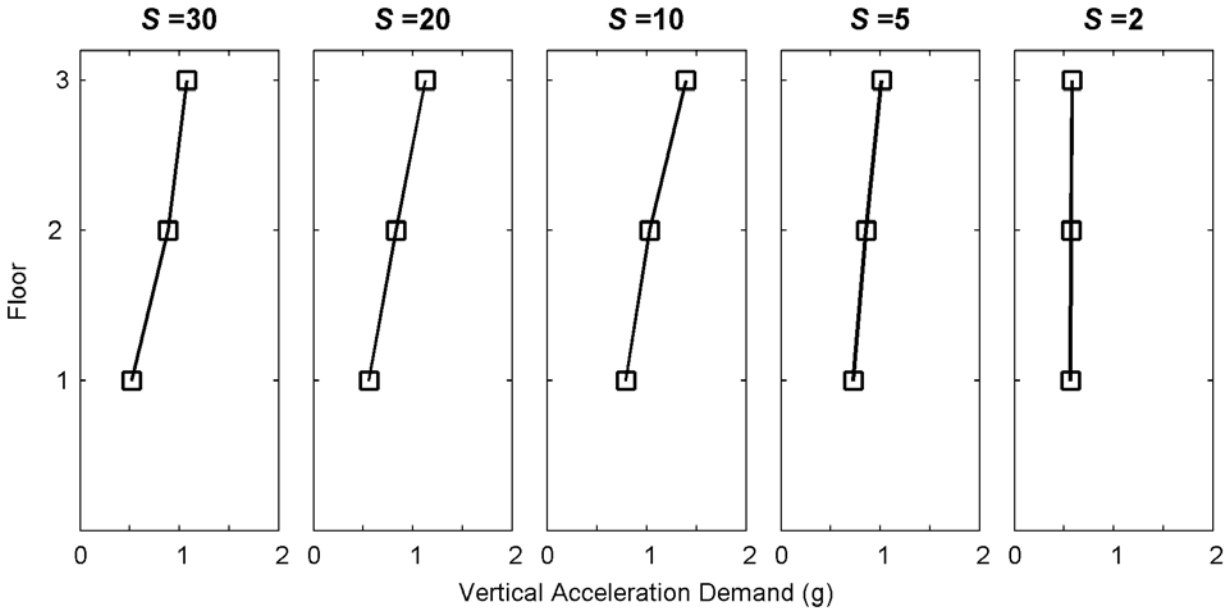

Figure 4.5. Average vertical acceleration demands in 3-story frame at each floor level

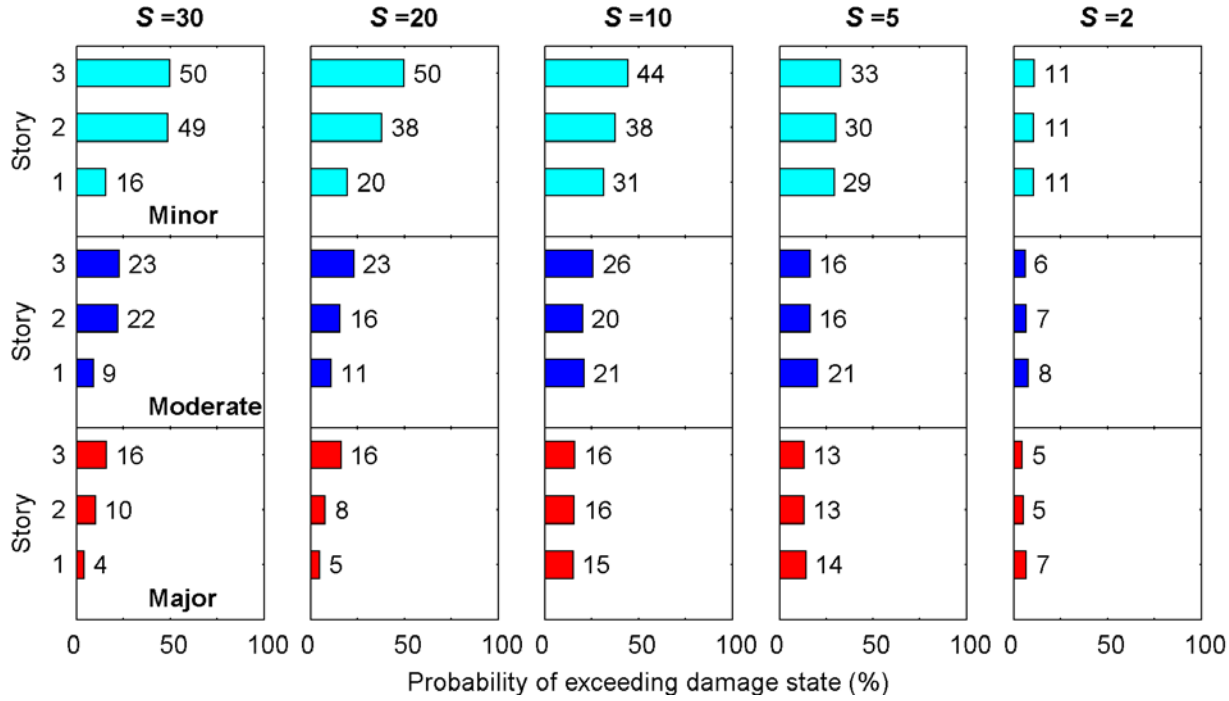

Figure 4.6. Probability of exceeding minor, moderate and major damage states for suspended ceiling systems in 3-story frame

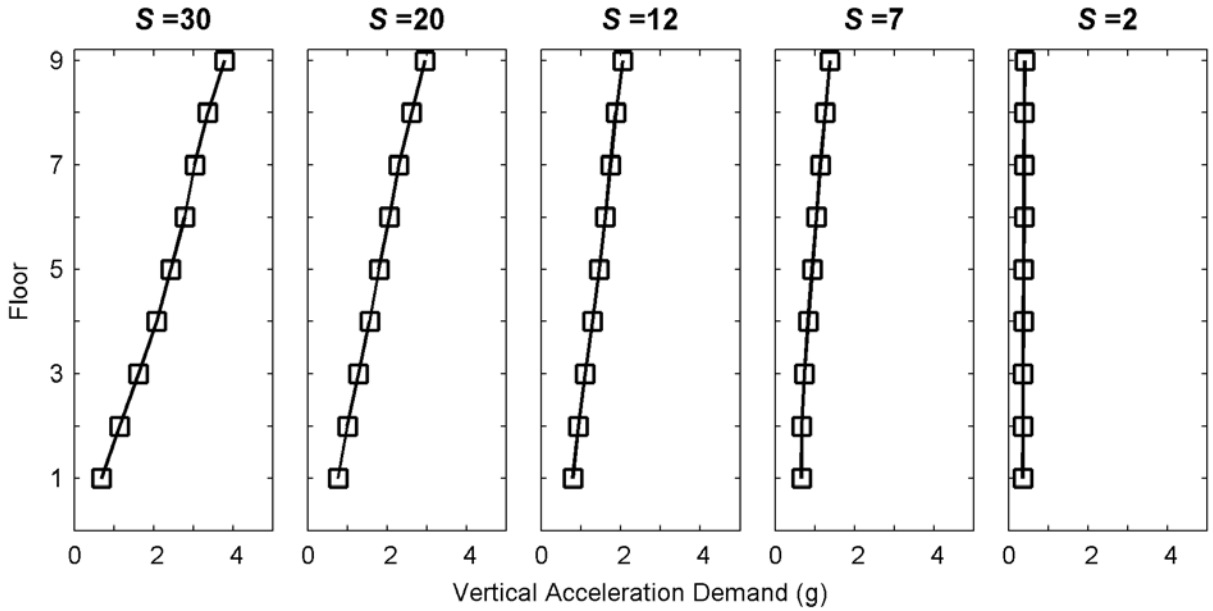

Figure 4.7. Average vertical acceleration demands in 9-story frame at each floor level

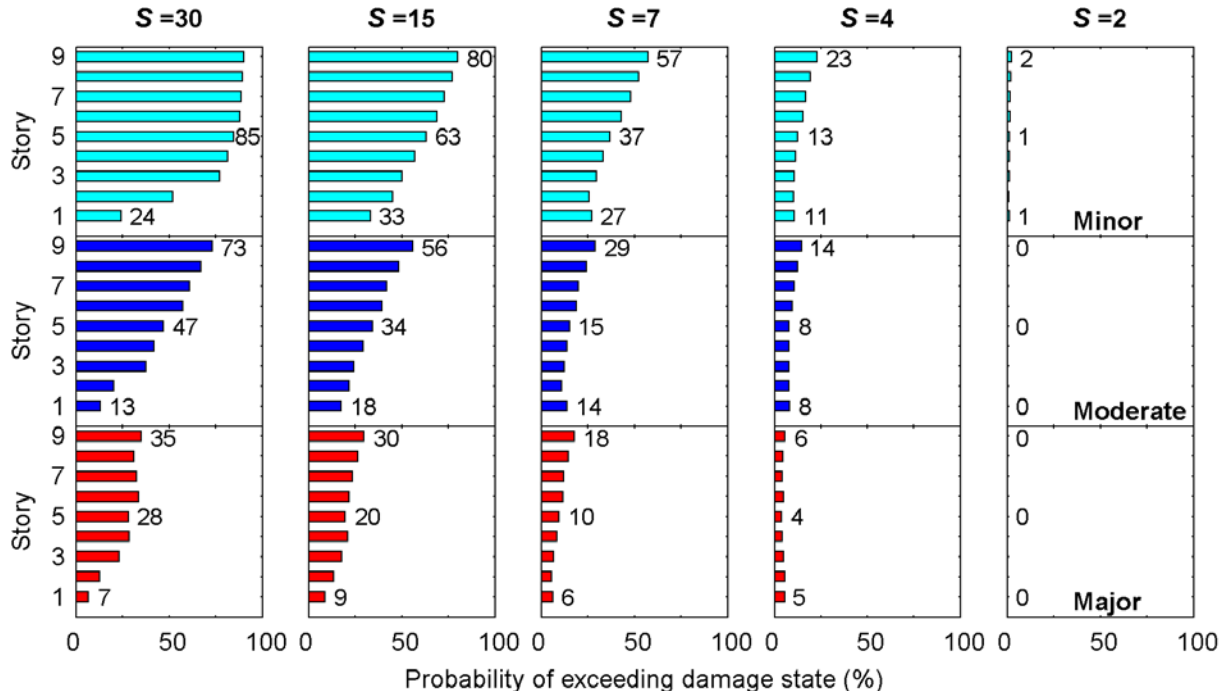

Figure 4.8. Probability of exceeding minor, moderate and major damage states for suspended ceiling systems at 9-story frame

Due to the large vertical acceleration demands at the roof level, the probability of failure of the ceiling systems is highest at that level. For the 3-story frame (Fig. 4.6), the probability of having minor failure at the roof ranges from 50% for S = 30 to 11% for S = 2. The probability of

having major damage is much smaller which ranges from 16% for S = 30 to 5% for S = 2. For the 9-story frame (Fig 4.8), the probability of having minor failure at the roof ranges from 90% for S = 30 to 2% for S = 2, and the probability of having major damage ranges from 35% for S = 30 to 0% for S = 2. The results plotted in Figs. 4.6 and 4.8 suggest that using low shape factors ($S \leq 2$) effectively mitigates damage to ceiling systems in both 3- and 9-story frame. However, low shape factor bearings have practical limitations as discussed in the subsequent section.

4.2.3 Stability and rocking limitations

As illustrated in Figs. 4.4a and 4.4b, isolation systems composed of bearing with low shaper factor (e.g., S = 1 or 2) effectively limit vertical acceleration demands and thus limit the likelihood of damage to suspended ceilings as shown in Figs. 4.6 and 4.8. However, stability limit of the individual bearings and global rocking limit of the structure must be considered. To identify the lowest shape factor that could practically be implemented, the stability of the individual bearing in both the 3-story and 9-story frames were assessed using the current methodology (as described in Chapter 2). Figure 4.9 presents a graphical plot of the stability assessment for the 3-story frame and each isolation system considered. In this plot, the vertical load demands at a given lateral displacement (shown by various symbols) are compared to the predicted capacity of the bearing using the reduced area method (shown by the solid line). Vertical load demands falling above the capacity of the bearing indicate systems that do not satisfy the stability criteria. From Fig. 4.9, for the 3-story frame, it can be seen that isolation systems with $S < 5$ do not satisfy the stability criteria and therefore are not feasible. For the 3-story frame the lowest practical shape factor that could be used is S=5. Figure 4.10 presents the stability assessment for the individual bearings in the 9-story frame. From the results plotted in this figure the lowest shape factor that satisfies the stability criteria is S=7. Therefore, while the lower shape factors reduce the likelihood of damage (see Figs. 4.6 and 4.8) they do not satisfy the stability criteria according to current stability requirements (AASHTO 2010) and are not feasible.

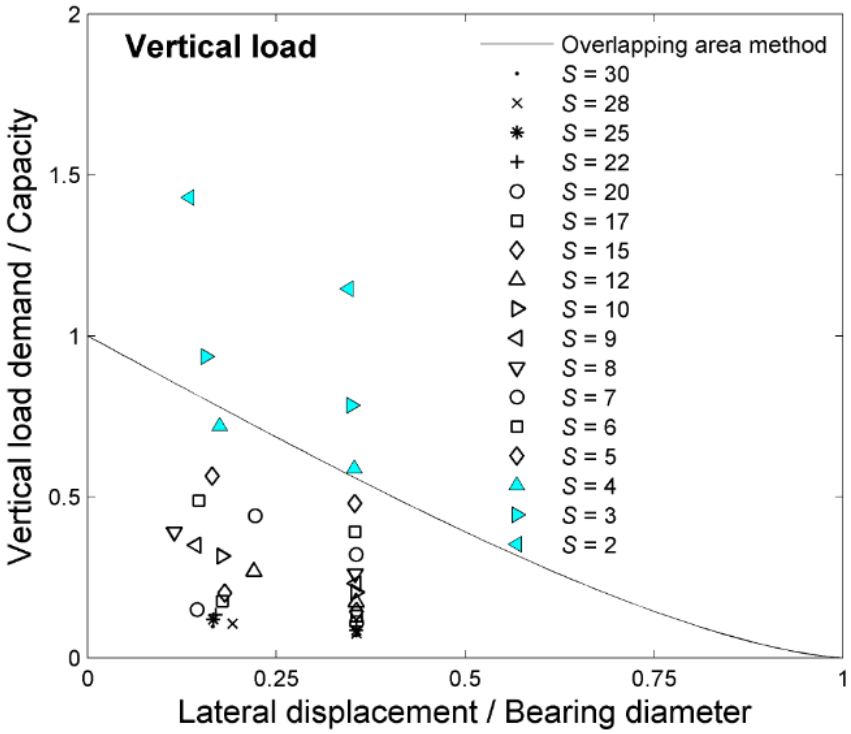

Figure 4.9. Feasible shape factor for 3-story frame

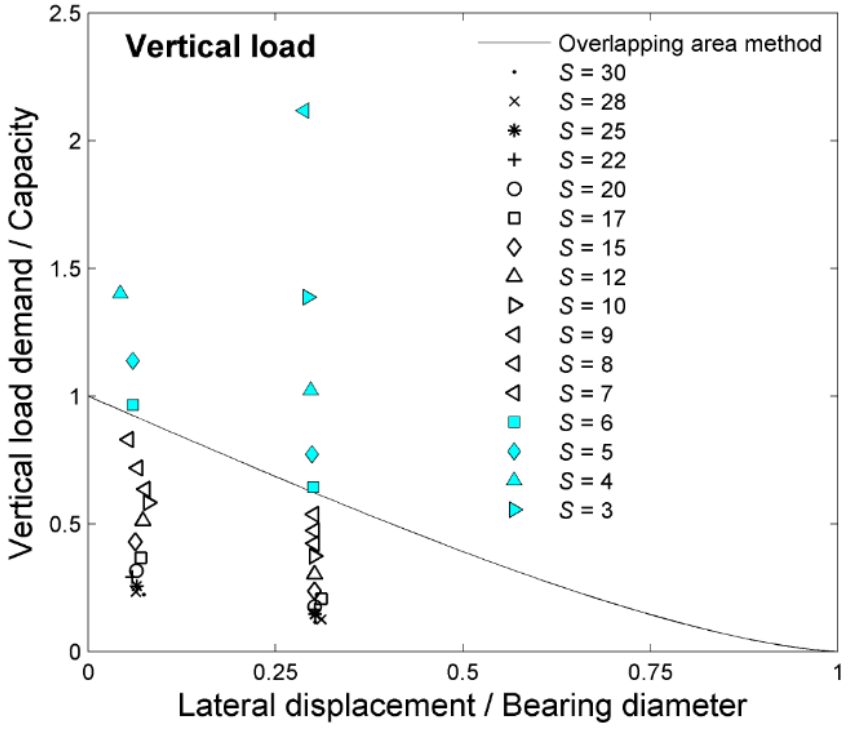

Figure 4.10. Feasible shape factor for 9-story frame

In addition to the stability assessment, the global drift or rocking of the superstructure needs to be considered. In this study, rocking is assessed using the global drift ratio of the superstructure that is the drift between the roof and base of the superstructure (excludes isolation drift) divided by the total height of the superstructure. The global drift demands were then compared to the widely accepted 2 percent value to determine the suitability of a particular isolation system. Figure 4.11 presents peak global drift ratios versus isolation system shape factor for the 3-story (Fig. 4.11a) and 9-story (Fig. 4.11b) structures. Plotted in each figure are the drift ratio demands for each ground motion and shape factor for a given ground motion (denoted Individual) and the average of the individual drift demands. From the results presented in Fig. 4.11 the drift demands for all systems do not exceed 2% with a maximum value of 1.2. Although the drift demands do not exceed the 2% limit for any system, a significant increase in demand is observed for systems with shape factors less than or equal to 5. Based on these results a shape factor of 5 was considered as the rocking drift limitation for the 3-story and 9-story frames. For shape factors below 5, average peak drifts increased exponentially to the maximum value of 1% for a shape factor of 1. The results presented in Fig 4.11 also suggest that the shape factors need not be so high (i.e., greater than 20) to mitigate rocking in low- and mid-rise structures as drift ratio demands are essentially constant for $S > 5$.

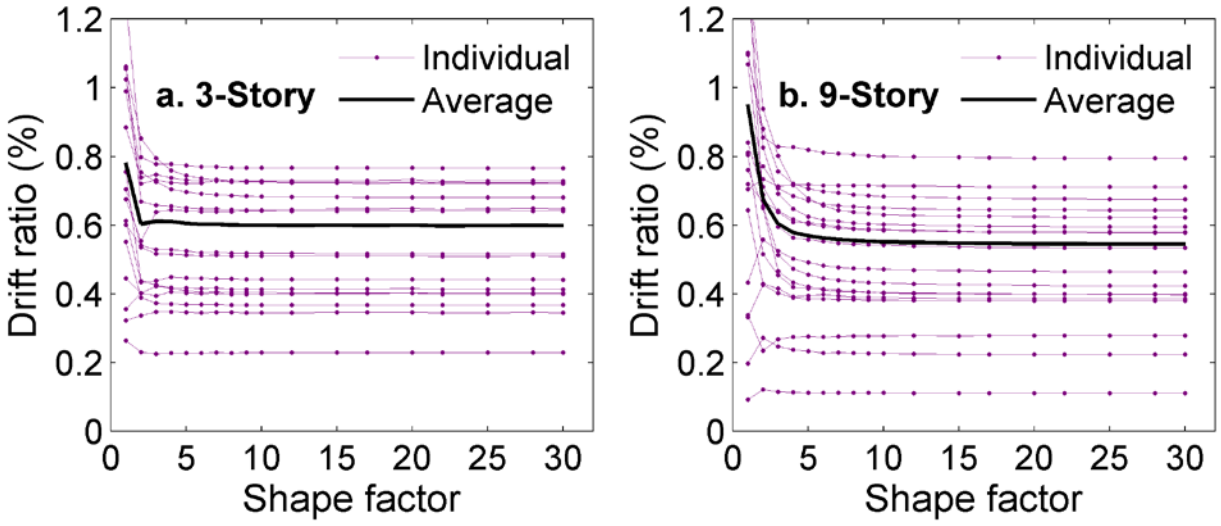

Figure 4.11. Peak drifts versus shape factor for frames with base isolation only: (a) 3-story; (b) 9-story

4.3 Results for base isolated frames with supplemental damping

A parametric study was conducted to investigate the influence of supplemental damping on acceleration demands and fragility of suspended ceilings in the upper levels of base isolated frames. Three values of the damping ratio were analyzed ranging from 0%, 10% and 20%.

4.3.1 Vertical acceleration demands

Figures 4.12 and 4.13 present the average peak vertical absolute acceleration demands at the base and roof of the 3- and 9-story frames, respectively with various supplemental damping ratios. Peak vertical absolute accelerations demand presented in Figs. 4.12 and 4.13 are the average of twenty peak demands at a particular level normalized by gravitational acceleration (g). Fig 4.12 and Fig 4.13 illustrate the influence of supplemental damping in reducing vertical acceleration demands in which supplemental damping ratios range from 0% - 20% of critical damping ratio. Results presented in Figs 4.12 and 4.13 show supplemental damping marginally reduces the vertical acceleration demands at the base and roof of both 3- and 9-story. From Fig 4.13b, at the roof there is significant amplification of the vertical acceleration for $S > 5$ regardless of the level of supplemental damping added at the base isolation level. From the results presented in Figs. 4.12 and 4.13, the lower vertical stiffness (i.e., smaller shape factor) systems effectively limit the peak vertical acceleration demands however other considerations such as rocking and bearing stability limit the value of the shape factor that can practically be used as is discussed in section 4.2.3.

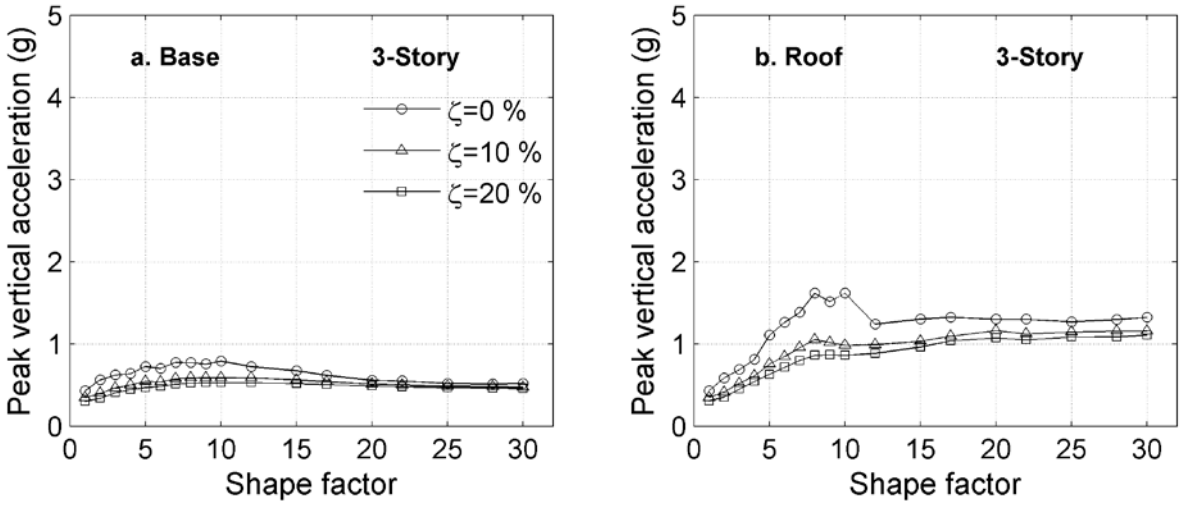

Figure 4.12. Average vertical acceleration demands in 3-story frame for various supplemental damping ratios: (a) base and (b) roof levels

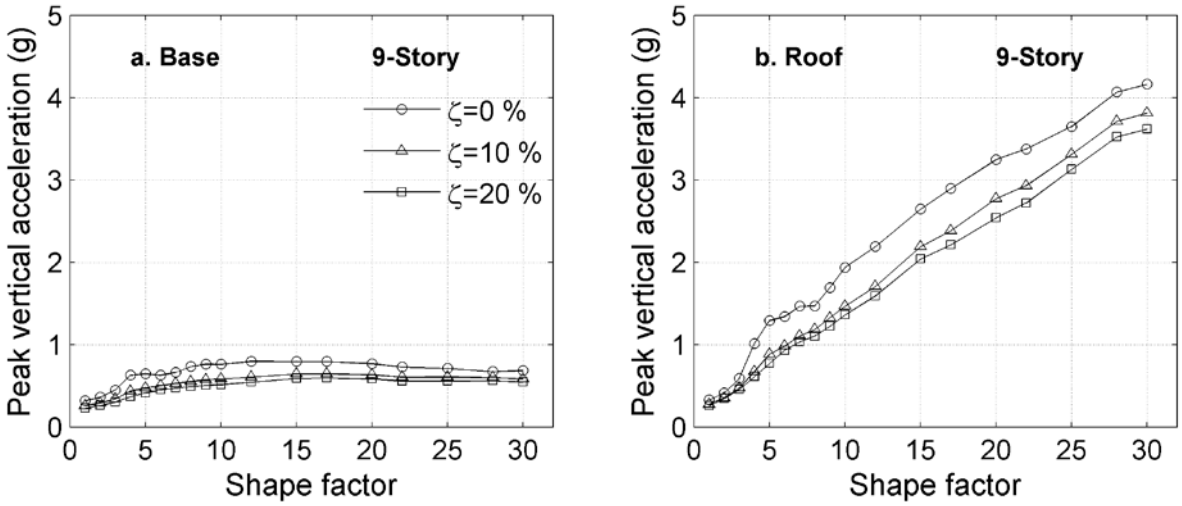

Figure 4.13. Average vertical acceleration demands in 9-story frame for various supplemental damping ratios: (a) base and (b) roof levels

4.3.2 Fragility of suspended ceilings

The probabilities of exceeding three damage states for various damping ratio are plotted in Figs. 4.14 and 4.15 for 3- and 9-story frames respectively. According to section 4.2.3 and assuming damping has no effect on vertical loads, the minimum feasible shape factors are S=5 for 3-story frame and S=7 for 9-story frame so that shape factors smaller than these numbers are no longer under consideration.

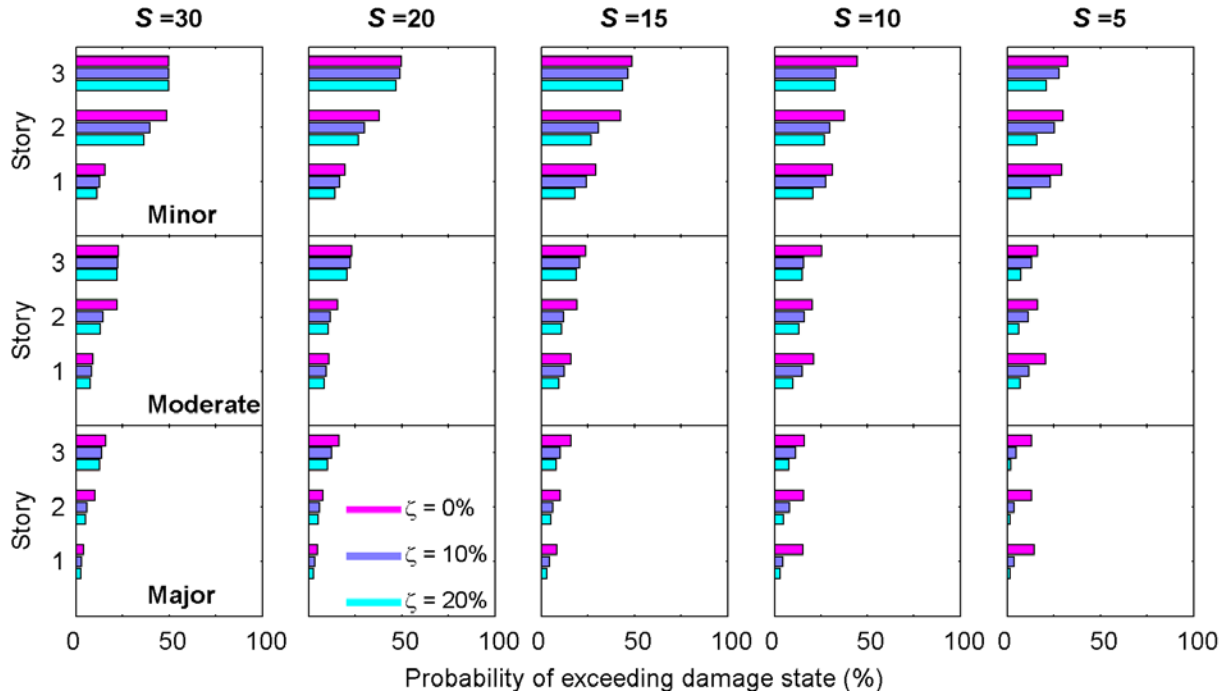

Figure 4.14. Probability of exceeding minor, moderate and major damage states for suspended ceiling systems at 3-story frame

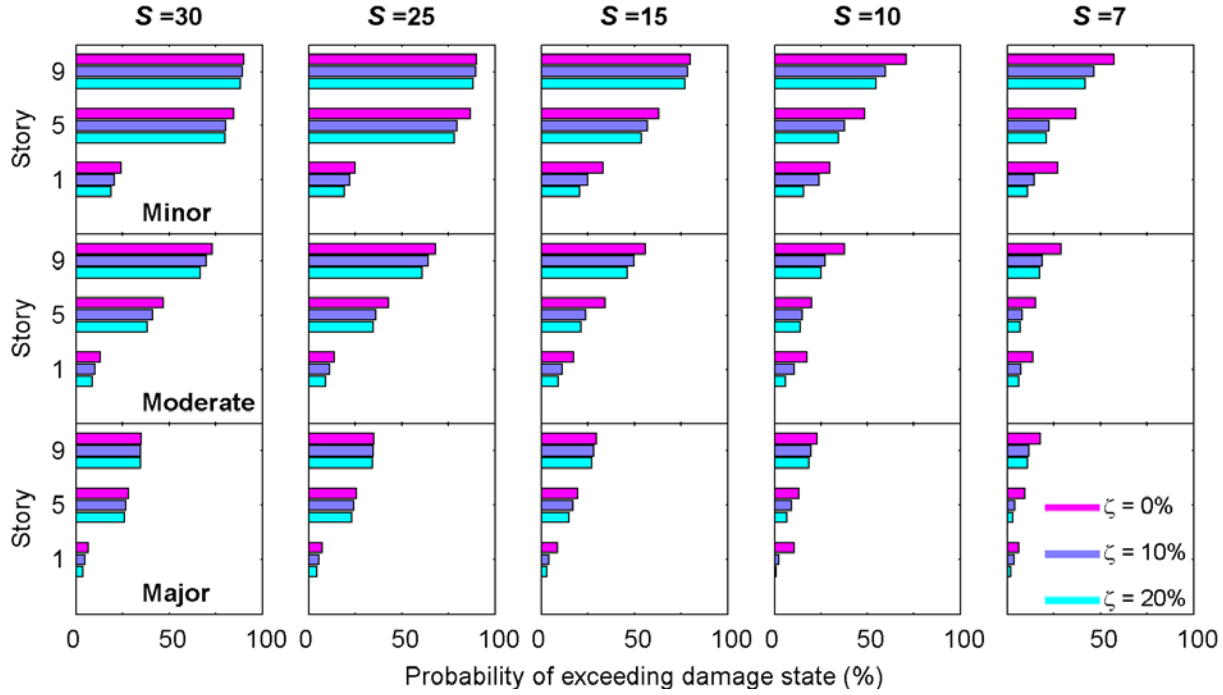

Figure 4.15. Probability of exceeding minor, moderate and major damage states for suspended ceiling systems at 9-story frame

The result presented in Figs. 4.14 and 4.15 suggested that adding supplemental damping for high shape factor bearing system is less beneficial compared to adding supplemental damping for low shape factor bearing. For shape factor S=30, the probability of exceeding damage for all three states are almost similar regardless of the level of supplemental damping added at the base isolation level. It can be explained as the large vertical stiffness (K_v) of high shape factor bearing restrains the damper from dissipating energy. Furthermore, the combination of moderate shape factor (S=5 for 3-story frame and S=7 for 9-story frame) with supplemental damping appear effective for preventing major damage occur to the ceiling systems.

4.4 Results for base isolated frames with column isolators

As shown in the previous sections of this chapter isolation systems composed of low shape factor bearing can reduce the likelihood of damage (especially major) to suspended ceiling systems in both the 3- and 9-story frames. However, due to the stability limit of the bearings, low shape factors, i.e., below 5 and 7, are not feasible. Recognizing this, an alternative strategy of employing multiple planes of vertical flexibility in the upper stories of the build is explored. A potential benefit of the vertically distributed flexibility is that a similar vertical period can be achieved (similar to the low shape factor systems) but minimize stability issues and rocking because the flexibility is not concentrated at the base but rather distributed along the height of the building. This section presents results from an analytical exploration of the vertical distributed flexibility concept also referred to as "base isolated with column isolation."

4.4.1 Stability and rocking considerations

The results of the response history analyses for the 3-story and 9-story frames with column isolators installed as described in Chapter 3 were evaluated to determine peak drift values. Since the column isolators were proportioned using stability criteria (see Chapter 3) it is assumed that stability of the column isolators has been satisfied a priori. Figure 4.16 presents peak drift at the roof of the 3- and 9-story frames with column isolators. Although the individual drift values different from those without column isolators (i.e. Fig. 4.11), the average drift values are similar to those shown in Fig. 4.11. Consideration of the stability of the base isolators indicated that the lower limit of feasible shape factors for the 3- and 9-story frames remain to be 5 and 7, respectively.

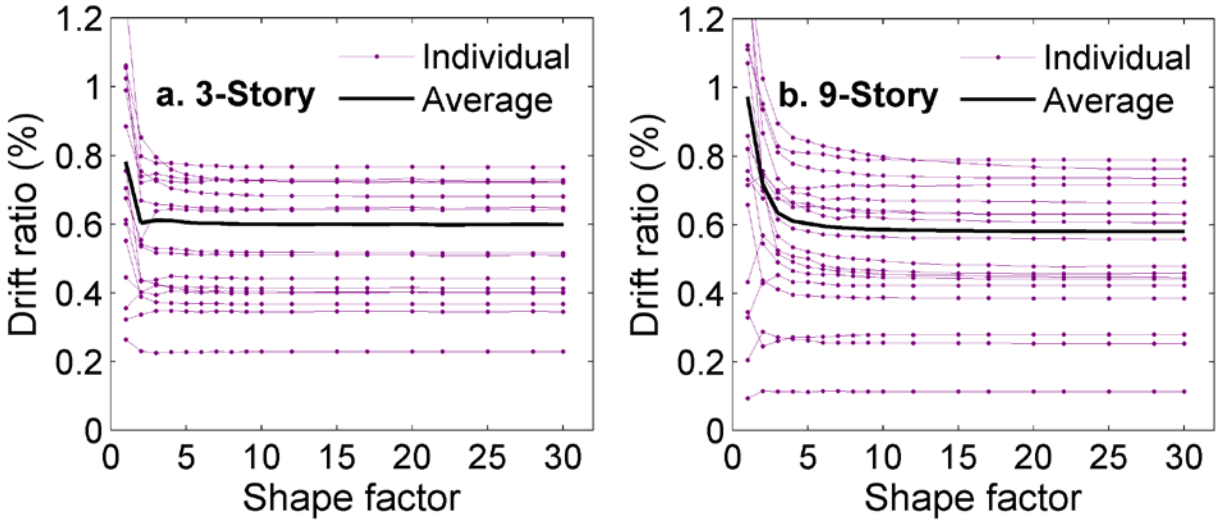

Figure 4.16. Peak drifts versus shape factor for frames with base isolation and column isolators: (a) 3-story; (b) 9-story

4.4.2 Vertical acceleration demands and fragility of suspended ceilings

Figure 4.17 presents a comparison of the average peak vertical acceleration demand in the base isolated 3-story frame with and without column isolators for base isolation systems with shape factors of 5, 15 and 30. The results presented in Fig. 4.17 show that the column isolators do not effectively reduce demands in the 3-story frame. Figure 4.18 presents vertical acceleration demands in the base isolated 9-story frame with and without column isolators. From the results presented in Fig 4.18, the benefit of the column isolators in terms of reducing vertical acceleration demands is most apparent for systems with high shape factors (i.e., S=30). Including the column isolators in the 9-story frame with S=30 reduced acceleration demands from approximately 4g at the roof to approximately 1.4g as shown in Fig. 4.18 with equally significant reduction for floors 3-8. Inversely, adding column isolators to low shape factor base isolation could lead to slight amplification in vertical acceleration demand (e.g., S = 7 for 9-story frame).

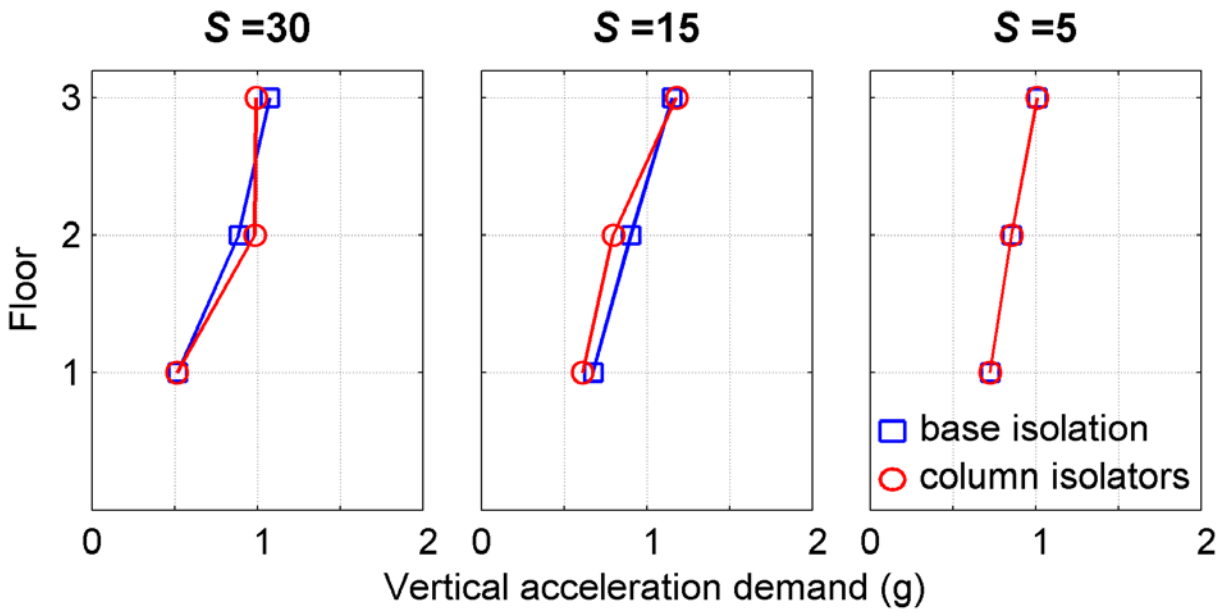

Figure 4.17. Comparison of vertical acceleration demands in 3-story frame with and without column isolators

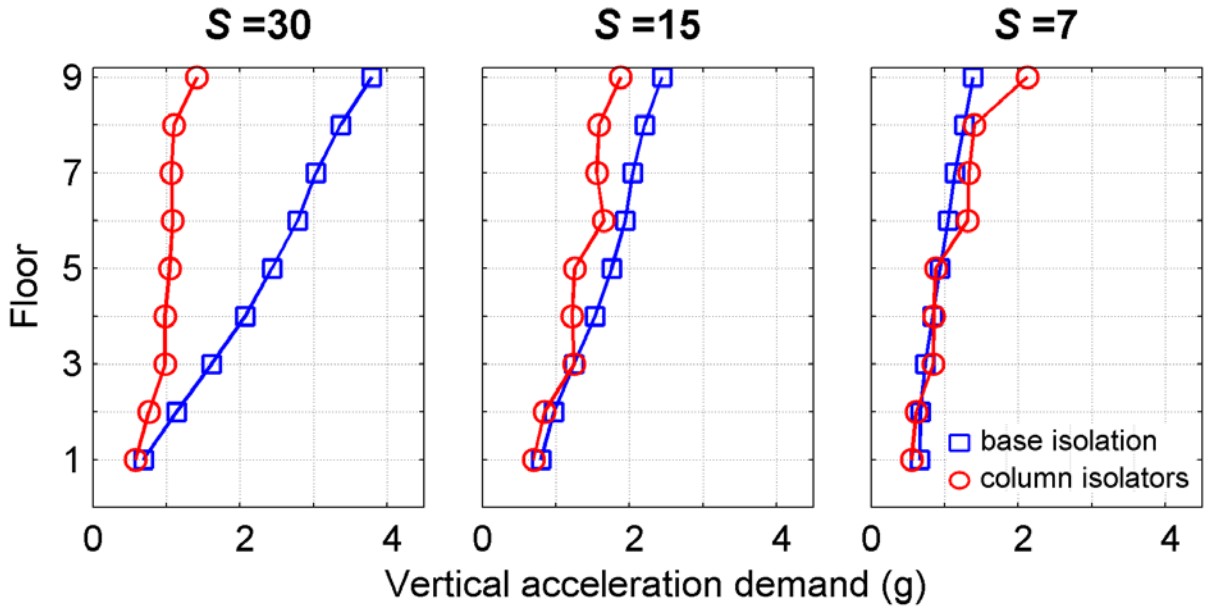

Figure 4.18. Comparison of vertical acceleration demands in 9-story frame with and without column isolators

Figure 4.19 presents a comparison of the probability of exceeding the minor, moderate and major damage states for suspended ceilings in the 9-story frame base isolated with *S*=30 (shape factor of base isolation) with (Fig. 4.19a) and without (Fig. 4.19b) column isolators. From

the comparison presented in Fig. 4.19 it can be seen that the column isolators effectively reduce the likelihood of major and moderate damage to the suspended ceiling system at the majority of the story levels.

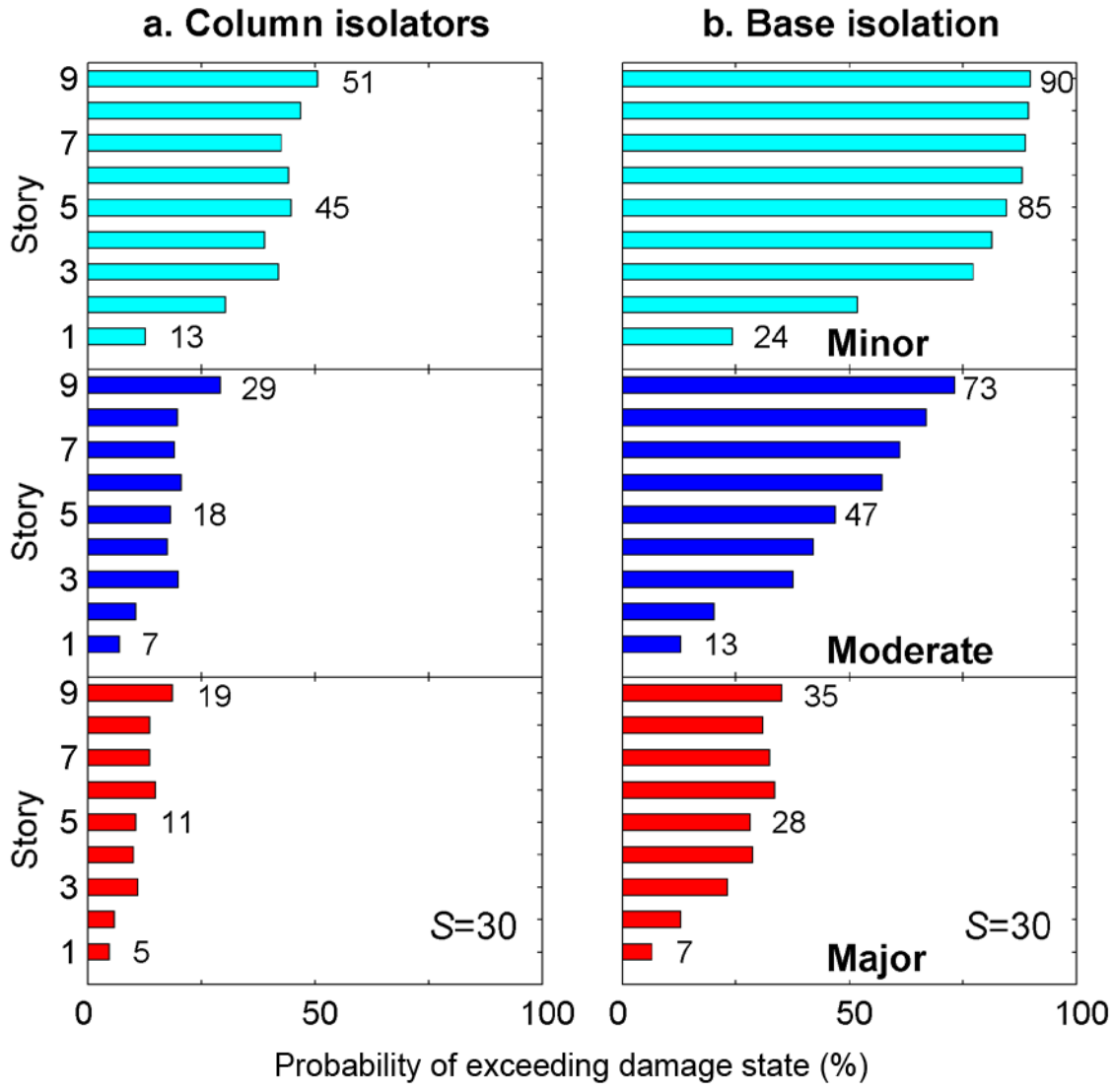

Figure 4.19. Comparison of the probability of exceeding damage states for the base isolated 9-story frame: (a) *S*=30 with column isolators; (b) *S*=30 without column isolators

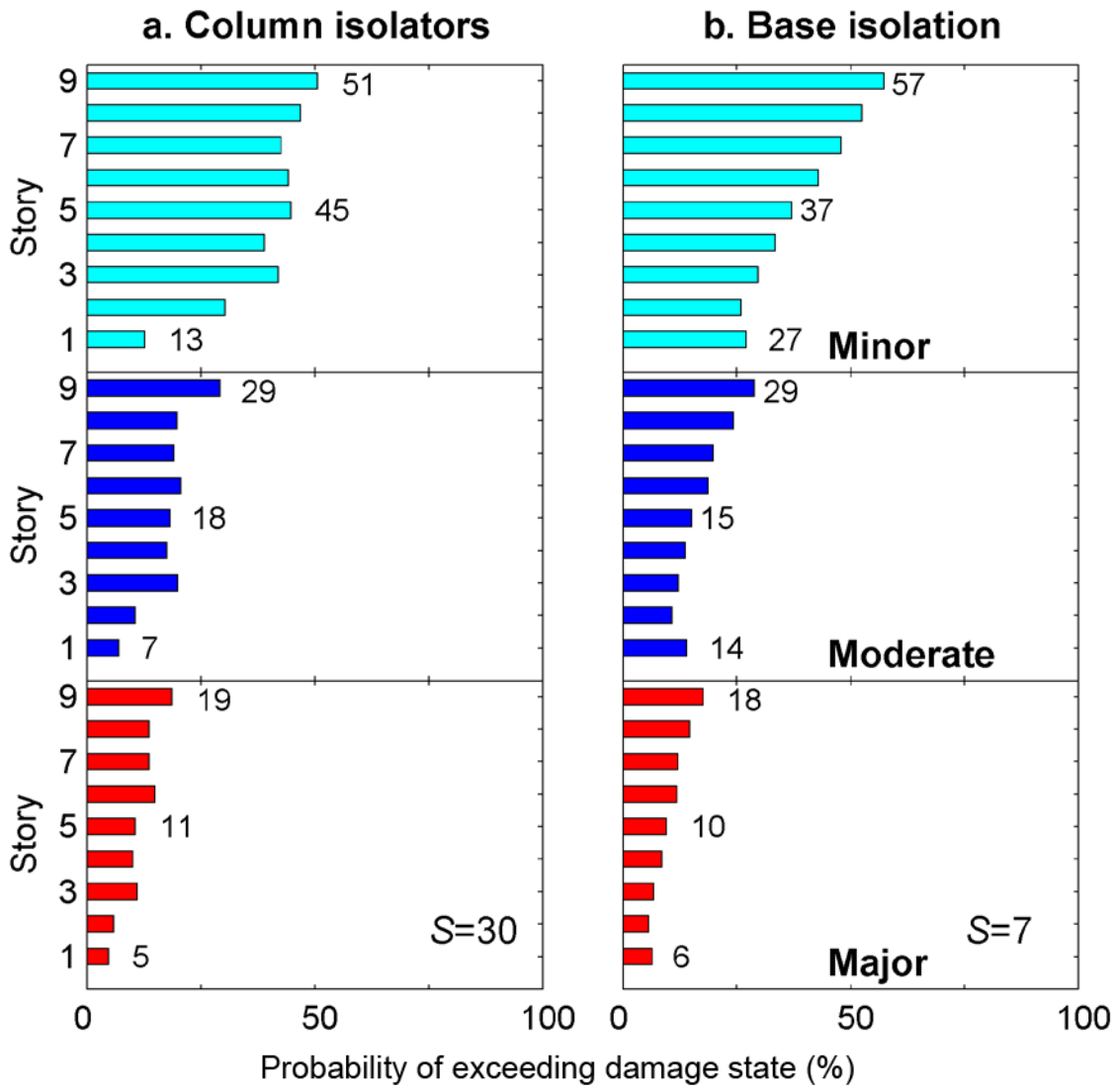

Figure 4.20. Comparison of the probability of exceeding damage states for the base isolated 9-story frame: (a) *S*=30 with column isolators; (b) *S*=7 without column isolator

Figure 4.20 compares the probability of exceeding minor, moderate and major damage states for the base isolated 9-story frame with S=30 and column isolators (Fig. 4.20a) versus a base isolation system with S=7 and no column isolators (Fig. 4.20b). From the results presented in Fig. 4.20, the column isolators reduces the probability of exceeding the minor, moderate and major damage limit states at all heights to less than 51% for minor damage, 29% for moderate damage and 19% for major damage. Comparing Fig 4.20a to 4.20b suggests that a base isolation system composed of high shape factor bearings combined with column isolators has an overall

similarity in performance i.e., reduced likelihood of damage, by comparison to a base isolation system composed of moderate to high shape factor bearings and no column isolators.

4.5 Summary

This section presented results of an analytical study aimed at exploring the concept of using low shape factor for base isolation and distributed flexibility up the height of structure via column isolators. From the results presented in this section, rocking (global drift) is not a limiting factor for $S > 5$ in these low and mid-rise buildings. Evaluation of the performance of the various systems using fragility data from suspended ceiling systems suggests the most effective strategy for minimizing damage to these systems in low-rise buildings could be the use of low shape factor bearing whereas in mid-rise buildings (i.e. 9-story) the combination of base isolators with high shape factors and column isolators appears to effectively reduce the likelihood of damage to suspended ceiling systems.

Chapter 5

Summary and conclusions

5.1 Summary

This research presents an analytical study of the two dimensional 3- and 9-story base isolated frame models subjected to earthquake excitation. The objectives of the research are to twofold: first to study the responses of different frame protective system configurations under seismic excitation, and second; to use fragility curves to estimate damage due to vertical component of earthquake ground shaking to ceiling systems in the structures. This estimation is used as a performance metric.

Twenty sets of ground motions used in this research are obtained from the Pacific Earthquake Engineering Research ground motion database (PEER 2011). Ground motions chosen have closest distance to rupture surface range from 0.96 km to 8.88 km and moment magnitude from 6.7 to 7.6. The frame models were analyzed for bi-axial excitations simultaneously in the horizontal and vertical directions.

Three and nine-story base isolated frames were developed and analyzed using OpenSees (2009). These frames were modified versions of the SAC buildings presented in Gupta and Krawinkler (1999). Three model configurations were considered in this research, specifically: base isolated frame; base isolation with supplemental damping; and base isolation with vertically distributed column isolators.

Fragility data from Badillo et al. (2006) was adapted to evaluate the probability of exceeding damage states of the ceiling systems in three model configurations. Fragility curves were generated from Badillo et al. (2006) study so that probability of failure is calculated for a wide range of vertical to horizontal acceleration demands. Three damage states were defined by Badillo to characterize the seismic performance of the ceiling systems, namely: minor damage, moderate damage and major damage.

5.2 Limitations of the study

Although the research has reached its objectives, there were some limitations. The availability of seismic fragility data for suspended ceilings in the public domain is limited. A

study by Badillo et al. (2006) provides fragility curves for suspended ceiling systems based on experimental testing. Each fragility data point used to construct the fragility curves was based in a small sample size (6 tests) so that confidence in the predictive capability of the curves is low. However, for this study the Badillo et al. data was used to evaluate and compare various systems rather than predicting an actual failure probability. Moreover, there have been a limited number of experimental tests on seismically isolated buildings included vertical excitation. This translates into a limited amount of data available to verify the analytical models used in this study. However, results from recent full-scale testing of a 5-story base isolated steel frame (Ryan et al. 2012) agree qualitatively with the results of the analytical models used in this study.

5.3 Conclusions

Based on the results presented in this thesis, following conclusions are provided:

- For the 2-dimensionl frame considered in this study, the limiting factor for the use of low shape factor bearing does not appear to be rocking, as measured by the global drift ratio, but rather stability of the individual bearings. Maximum drift ratios of approximately 1.2% were observed for bearings with shape factors equal to 1 though stability considerations limited the shape factor to greater than or equal to 7.
- Low shape factors (i.e. less than 5) effectively limited damage to suspended-ceiling systems, however stability considerations preclude the use of such low shape factors. Therefore the low shape factor approach to achieve three-dimensional protection is not feasible for low to mid rise buildings.
- The vertically distributed flexibility concept effectively reduced the likelihood of damage to suspended ceiling systems in the 9-story frame by comparison to a traditional base isolated frame on high shape factor bearings. The vertically distributed flexibility concept, however, was not effective for the 3-story frame by comparison to a traditional base isolated frame on high shape factor bearings. This suggest, a different approach is needed for low-rise buildings such as a vertically flexible bearing (i.e. $5 < S < 10$) with added supplemental damping to effectively protect suspended ceiling systems.

References

American Association of State Highways and Transportation Officials (AASHTO). (2010). "Guide specifications for seismic isolation design." AASHTO, Washington, DC.

Aiken, I. D., Kelly, J. M. and Tajirian, F. F. (1989). "Mechanics of low shape factor elastomeric seismic isolation bearings." *Report No. UCB/EERC-89/13*, Earthquake Engineering Research Center, University of California, Berkeley, CA.

American Association of State Highways and Transportation Officials (AASHTO). (2010). "Guide specifications for seismic isolation design." AASHTO, Washington, DC.

American Society of Civil Engineers (ASCE). (2010). "Minimum Design Loads for Buildings and other Structures." ASCE, Virginia 20191.

Badillo, H., Whittaker, A. S. and Reinhorn, A. M. (2006). "Seismic Fragility of Suspended Ceiling Systems." *Technical Report MCEER-06-0001*, State University of New York at Buffalo, Buffalo, New York.

Broderick, B. M., Elnashai, A. S., Ambraseys, N. N., Barr, J. J., Goodfellow, R. G. and Higazy, E.M. (1994). "The Northridge (California) earthquake of 17 January 1994: Observations, strong-motion and correlative response analyses." *Research Report ESEE-Y4/4*, Imperial College.

Bozorgnia, M. N. and Campbell, K. W. (1995). "Characteristics of free-field vertical ground motion during the Northridge earthquake." *Earthquake Spectra*, 23, 515-525.

Buckle, I. G. and Liu, H. (1994a). "Critical loads of elastomeric isolators at high shear strain." *Proc., 3rd U.S.-Japan Workshop on Earthquake Protective Systems for Bridges*, National Center for Earthquake Engineering Research, State Univ. of New York, Buffalo, NY.

Buckle, I. G. and Liu, H. (1994b). "Experimental determination of critical loads of elastomeric isolators at high shear strain." *NCEER Bull.*, 8(3), 1–5.

Chalhoub, M. and Kelly, J. M. (1990). “Effect of Bulk Compressibility on the Stiffness of Cylindrical Base Isolation Bearings.” *International Journal of Solids Structures*, 26, 743-760.

Chopra, K. A. (2006). “Dynamics of structures.” Prentice Hall. Upper Saddle River, New Jersey.

Dao, N., Ryan, K.L., Siavash, S., Manos, M., Eiji, S., Tomohiro, S. and Arash, Z. (2011). “Experimental evaluation of an innovative isolation system for a lightweight steel moment frame building at E-Defense.” *Proc., ASCE Structures Congress*, Las Vegas, NV.

Derham, C. J. and Thomas, A. G. (1981). “The design of seismic isolation bearings.” Control of seismic response of piping systems and other structures by base isolation, Univ. of California, Berkeley, CA, 21–36.

Gent, A. N. (1964). “Elastic stability of rubber compression springs.” *J. Mech. Eng. Sci*., 6(4), 318–326.

Goltz, J. D. (1994). “The Northridge, California earthquake of January 17, 1994 General reconnaissance report.” *Technical Report NCEER-94-0005*.

Gupta, A. and Krawinkler, H. (1999). “Seismic demands for performance evaluation of steel moment resisting frame structures.” *Report no. 132*. John A. Blume Earthquake Engineering Center, Stanford University, Paolo Alto, CA.

Hall, J. F. (1995). “Northridge earthquake reconnaissance report.” *Earthquake Spectra*, Supplement C to Volume 11.

Haringx, J. A. (1948). “On highly compressible helical springs and rubber rods and their application for vibration-free mountings. I.” *Philips Res. Rep*., 3, 401–449.

Haringx, J. A. (1949a). “On highly compressible helical springs and rubber rods and their application for vibration-free mountings. II.” *Philips Res. Rep*., 4, 49–80.

Haringx, J. A. (1949b). “On highly compressible helical springs and rubber rods and their application for vibration-free mountings. III.” *Philips Res. Rep*., 4, 206–220.

Hilmy, S. I. and Masek, J. P., (1994). “Failure mechanisms of parking structures damaged during the Northridge earthquake, January 17, 1994.” *Special Report*, Dames & Moore Structural/Earthquake Engineering Group.

HITEC (1998a). “Evaluation findings for Skellerup base isolation elastomeric bearings.” Civil Engineering Research Foundation, Washington, D.C.

HITEC (1998b). “Evaluation findings for Dynamic Isolation Systems, Inc. elastomeric bearings.” Civil Engineering Research Foundation, Washington, D.C.

Huffmann, G. (1984). “Full base isolation for earthquake protection by helical springs and visco dampers.” *Nuclear Engineering and Design*, 331-338.

IBC 2000. “International Building Code.” International Code Council, Country Club Hills, Ill, USA, 2000.

Kageyama, M., IBA, T., Somaki, T. and Hisako, H. (2002). “Development of cable reinforced 3-dimensional base isolation air spring.” *ASME Pressure Vessels and Piping Conference*, Vancouver, Canada.

Kageyama, M., IBA, T., Somaki, T., Moro, S., Shinya, I. and Hisako, H. (2004). “Study on three dimensional seismic isolation system for next generation nuclear power plant: independent cable reinforced rolling-seal air spring.” *13th World Conference on Earthquake Engineering*, August 1-6, 2004, Vancouver, Canada.

Kelly, J. M. (1997). “Earthquake-Resistant Design with Rubber.” Springer Publishing Company, New York 10036.

Makris, N. and Deoskar, H. S. (1996). “Prediction of observed response of base-isolated structure.” *Journal of Structural Engineering*, vol. 122, no. 5, pp. 485–492.

Mokha, A., Constantinou, M. C. and Reinhorn, A. M. (1990a). "Experimental study and analytical prediction of earthquake response of a sliding isolation system with a spherical surface." *Report No. NCEER-90-0020*, Nat. Ctr. for Earthquake Engineering. Res., State Univ. of New York, Buffalo, N.Y.

Mokha, A., Constantinou, M. C. and Reinhorn, A. M. (1990b). "Teflon bearings in base isolation. I: Testing." *Structural Engineering*, ASCE, 116(2), 438-454.

Open system for earthquake engineering simulation framework (OpenSees). (2009). Version 2.3. Pacific Earthquake Engineering Research Center, University of California, Berkeley. (http://opensees.berkeley.edu/).

Papazoglou, A. J. and Elnashai, A. S. (1996). "Analytical and field evidence of the damaging effect of vertical earthquake ground motion." *Earthquake Engineering and structural dynamics*, Vol. 25, 1109-1137.

PEER (2011). PEER NGA Database, Pacific Earthquake Engineering Research Center, University of California, Berkeley, CA: http://peer.berkeley.edu/peer_ground_motion_database/

Reitherman, R. (1995). "Nonstructural Damage" *Earthquake Spectra*, Supplement to Volume 11, Northridge Earthquake Reconnaissance Report, Earthquake Engineering Research Institute, Oakland, California.

Ryan, K.L., Dao, N., Siavash, S., Manos, M., Eiji, S., Tomohiro, S. and Arash, Z. (2012). "Seismic Interaction of Structural System and Non-structural Components in the NEES TIPS/NEES Nonstructural/NIED Collaborative Tests at E-Defense." *Proc. 2012 ASCE Structures Congress*, Chicago, IL.

Sanchez, J., Masroor, A., Mosqueda, G. and Ryan, K. (2011). "Static and Dynamic Stability of Elastomeric Bearings for Seismic Protection of Structures." *Journal of Structural Engineering*, doi: 10.1061/(ASCE)ST.1943-541X.0000660

Sasani, M. and Kiureghian, A. (2001). "Seismic Fragility of RC Structural Walls: Displacement Approach." *Journal of Structural Engineering*, Vol. 127, No.2, pp. 219-228.

Sato, E., Furukawa, S., Kakehi, A. and Nakashima, M. (2011). "Full-scale shaking table test for examination of safety and functionality of base-isolated medical facilities." *Earthquake Engineering and Structural Dynamics*, 40, 1435-1453.

Sato, E., Kajiwara, K., Furukawa, S., Ji, X. and Nakashima, M. (2010). “Full-Scaled Shaking Table Test of a Hospital Made of Base-Isolated Four-Story Concrete Structure.” *Proceedings from the 9th US National and 10th Canadian Conference on Earthquake Engineering*, Toronto, CA.

Soroushian, S., Ryan, K.L., Maragakis, M., Sato, E., Sasaki, T., Okazaki, T., Tedesco, L., Zaghi, A.E., Mosqueda, G., Alvarez, D. (2012). “Seismic response of ceiling/sprinkler piping nonstructural systems in NEES TIPS / NEES Nonstructural /NIED collaborative tests on a full scale 5-story building.” *Proc. 2012 ASCE Structures Congress*, Chicago, IL.

Takahashi, O., Hiromasa, A., Junji, S., Ryoichiro, M., Yasuo, T. and Takafumi, F. (2008). “Construction of Civil Building using three dimensional seismic isolation system.” *The 14th World Conference on Earthquake Engineering*, October 12-17, 2008, Beijing, China.

Tajirian, F.F., Kelly, J. M., Aiken, I.D., and Veljovich, W. (1990). “Elastomeric Bearings for Three-Dimensional Seismic Isolation.” *Proc. of the 1990 ASME PVP Conference*, Nashville, Tennessee, June.

Tetsuya, H., Junji, S. and Satoshi, M. (2004). “Three-Dimensional Seismic Isolation Device with Rolling Seal Type Air Spring.” *ASME Conf. Proc*, 2004, 43.

Weisman, J. and Warn, G. (2012). “Stability of elastomeric and lead-rubber seismic isolation bearings.” *Journal of Structural Engineering*, 138(2), 215-223.

Yoo, B., Lee, J. H., Koo, G. H. and Kim, Y. H. (1997). “A study of vertical seismic responses for base isolated PWR using high damping rubber bearing.” *14th International conference on Structural Mechanics in Reactor Technology*, Lyon, France.

Appendix A

Basic loading conditions

The loading information was provided as follow:

Steel framing:	13 psf
Roofing:	7 psf average
Ceilings/Flooring:	3 psf average, including fireproofing
Mechanical/Electrical:	7 psf average for all floors, additionally 40 psf over penthouse area for equipment
Partitions:	10 psf for seismic load, 20 psf for gravity design
Exterior Wall:	25 psf of wall surface average, including any penthouses.
Live Load:	50 psf
Wind Load:	exposure B as per UBC 1994 definition

Appendix B

Description of ground motion

Ground motions representative of different hazard levels have been assembled in Bin 1 for this research. All these ground motions are assembled from The Pacific Earthquake Engineering Research Center (PEER 2011) ground motion database as it includes a very large and comprehensive set of ground motions recorded worldwide. Bin 1 consisted of recorded ground motions representing return period of 2474 years (2% probability of being exceeded in 50 years). Bin 1 of ground motions consists of 30 time histories; 10 ground motions each with 2 orthogonal horizontal components and 1 vertical components. Table B.1 provides fundamental information for the individual earthquake records constituting bin of ground motions.

Table B.1 Characteristic of ground motion records

Earthquake	Year	Moment Magnitude	Station	Compo nent	PGA (g)	Distance to Fault (km)	Site Class (USGS)	Mechanism
Kocaeli,Turkey	1999	7.4	Izmit	Up	0.146	7.21	A	SS
Kocaeli,Turkey	1999	7.4	Izmit	000	0.152	7.21	A	SS
Kocaeli,Turkey	1999	7.4	Izmit	090	0.22	7.21	A	SS
NorthRidge	1994	6.7	24207 Pacoima Dam (upper left)	Up	1.229	7.01	A	RN
NorthRidge	1994	6.7	24207 Pacoima Dam (upper left)	000	1.585	7.01	A	RN
NorthRidge	1994	6.7	24207 Pacoima Dam (upper left)	090	1.285	7.01	A	RN
Cape Mendocino	1992	7.1	89005 Cape Mendocino	Up	0.754	6.96	A	RN
Cape Mendocino	1992	7.1	89005 Cape Mendocino	000	1.497	6.96	A	RN
Cape Mendocino	1992	7.1	89005 Cape Mendocino	090	1.039	6.96	A	RN
Tabas, Iran	1978	7.4	9101 Tabas	Up	0.688	2.05	A	RN
Tabas, Iran	1978	7.4	9101 Tabas	000	0.836	2.05	A	RN
Tabas, Iran	1978	7.4	9101 Tabas	090	0.852	2.05	A	RN
Loma Prieta	1989	6.9	57180 Los Gatos- Lexington Dam	Up	0.536	5.02	A	RO
Loma Prieta	1989	6.9	57180 Los Gatos- Lexington Dam	000	0.515	5.02	A	RO
Loma Prieta	1989	6.9	57180 Los Gatos- Lexington Dam	090	0.367	5.02	A	RO
Loma Prieta	1989	6.9	58065 Saratoga - Aloha Ave	Up	0.389	8.50	B	RO
Loma Prieta	1989	6.9	58065 Saratoga - Aloha Ave	000	0.512	8.50	B	RO
Loma Prieta	1989	6.9	58065 Saratoga - Aloha Ave	090	0.324	8.50	B	RO
Kobe	1995	6.9	0 KJMA	Up	0.343	0.96	B	SS
Kobe	1995	6.9	0 KJMA	000	0.821	0.96	B	SS
Kobe	1995	6.9	0 KJMA	090	0.599	0.96	B	SS
NorthRidge	1994	6.7	LA Dam	Up	0.424	5.92	B	RN
NorthRidge	1994	6.7	LA Dam	000	0.511	5.92	B	RN
NorthRidge	1994	6.7	LA Dam	090	0.349	5.92	B	RN
Chi-Chi, Taiwan	1999	7.6	TCU089	Up	0.191	8.88	B	RN
Chi-Chi, Taiwan	1999	7.6	TCU089	000	0.333	8.88	B	RN
Chi-Chi, Taiwan	1999	7.6	TCU089	090	0.248	8.88	B	RN
Chi-Chi, Taiwan	1999	7.6	CHY080	Up	0.724	2.69	B	RN
Chi-Chi, Taiwan	1999	7.6	CHY080	000	0.968	2.69	B	RN
Chi-Chi, Taiwan	1999	7.6	CHY080	090	0.902	2.69	B	RN

Appendix C

Push over analysis

In this study, push-over analysis for 3- and 9-story frame has been carried out using the designed load pattern suggest in the ASCE 7-10. The governing equation for the load pattern is given as:

$$C_x = \frac{w_x h_x}{\sum_{i=1}^{n} w_i h_i} \tag{C.1}$$

where C_x is the normalized load at floor level x, w_i and w_x are the seismic weights at floor i and x respectively, h_i and h_x are the heights from the ground level to floor i and x. The push-over plots, i.e., the normalized base shear (base shear normalized by structure seismic weight, or V/W) versus roof drift angle (roof displacement normalized by structure height) response for the 3- and 9-story models are shown in Fig C.1a and C.1b respectively.

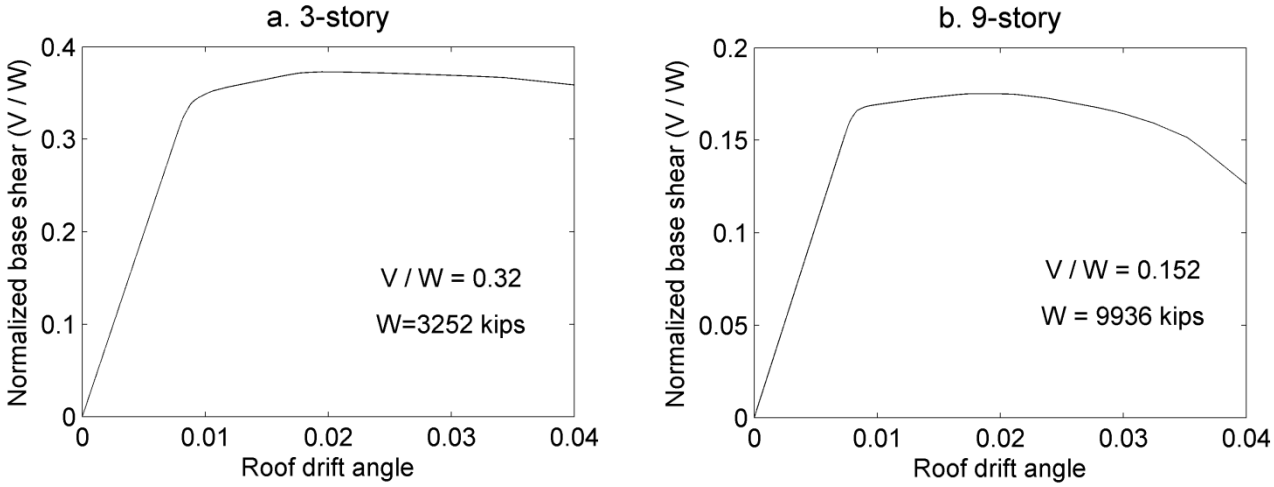

Figure C.1. Push over analysis for: (a) 3-story and (b) 9-story

Appendix D

Elastomeric bearings properties

In this research, elastomeric bearings were assumed to have bi-linear lateral and vertical force-deformation behavior to account for rubber inherent damping (Fig. D.1). 10 percent inherent damping in both lateral and vertical direction was chosen to represent moderate damping rubber bearings. Tables D.1 to D.3 below provide information to construct elastomeric bearings for 3- and 9-story frame.

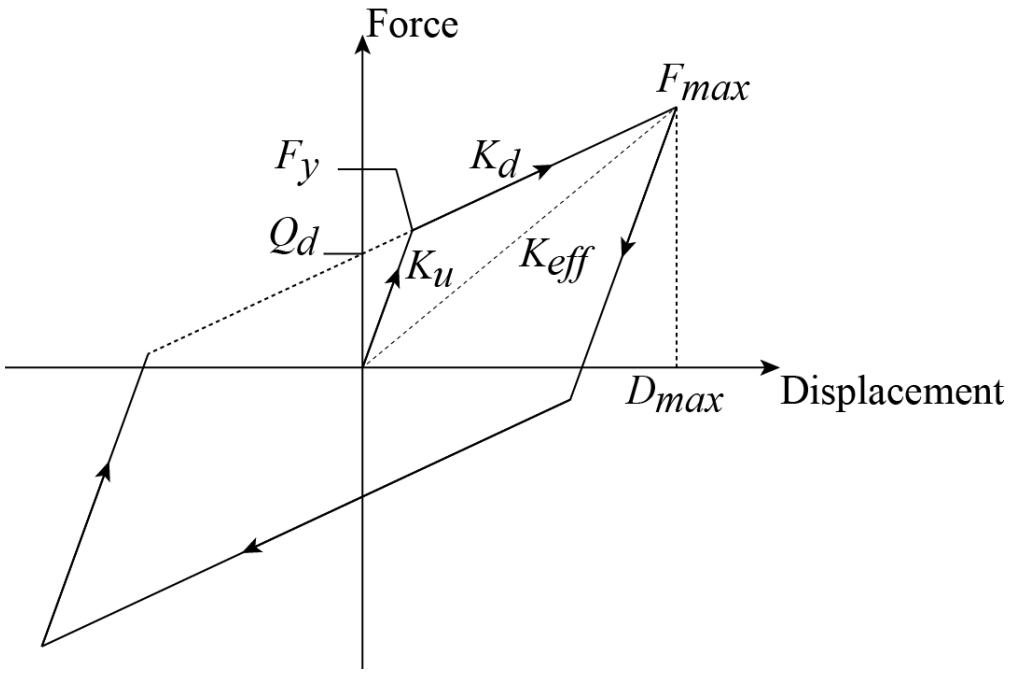

Figure D.1. Bilinear force-deformation characterization for elastomeric bearing

A sample calculation to design bearing isolators for 3-story frame

$$T_D \geq \frac{S_{D1}W}{R_I B_D V_S} = \frac{0.84 \times 3954}{1.5 \times 1.2 \times (3252 \times 0.32)} = 1.8\,\text{s}$$

Choose $T_D = 2\,\text{s}$

$$D_d = \frac{386.4 \times 0.84 \times 2}{4\pi^2 \times 1.5} = 13.7 \text{ in}$$

Assuming static pressure $p = 0.5$ ksi for all cases,

$$A = \frac{W}{p} = \frac{3954}{0.5} = 7908 \text{ in}^2$$

Total thickness of rubber (T_r) required:

$$T_r = \frac{GA}{K_{eff}} = \frac{0.1 \times 7908}{101} = 7.83 \text{ in}$$

Choose $T_r = 8$ in

Recalculate $K_{eff} = \frac{GA}{T_r} = \frac{0.1 \times 7908}{8} = 99$ (kips/in)

Distribute total horizontal stiffness to individual interior and exterior bearing isolators:

$K_{eff}^{exterior} = 12.4$ kips/in

$K_{eff}^{interior} = 24.7$ kips/in

Proportion lateral characteristic parameter for 3-story exterior base isolator:

$K_{eff}^{exterior} = 12.4$ kips/in; $D_d = 13.7$ in

Assuming yield displacement $Y = 0.1 D_d$ and inherent horizontal damping ratio is 10 %

$$Q_d = \frac{\pi \times \xi \times K_{eff} \times D_d^2}{2(D_d - Y)} = \frac{\pi \times 0.1 \times 12.4 \times 13.7^2}{2 \times (13.7 - 1.37)} = 29.6 \text{ kips/in}$$

$$K_d = K_{eff} - \frac{Q_d}{D_d} = 12.4 - \frac{29.6}{13.7} = 10.2 \text{ kips/in}$$

$$F_y = Q_d + K_d Y = 29.6 + 10.2 \times 1.37 = 43.5 \text{ kips}$$

$$K_u = \frac{F_y}{Y} = \frac{43.5}{1.37} = 31.8 \text{ kips/in}$$

Table D.1 Lateral characteristic of elastomeric bearings for 3 and 9-story frame

	K_{eff} (kips/in)		Q_d (kips/in)		K_d (kips/in)		F_y (kips)		K_u (kips/in)	
	exterior	interior	exterior	interior	exterior	interior	exterior	interior	exterior	interior
3-story	12.4	24.7	29.6	59.1	10.2	20.4	43.5	87	31.8	63.5
9-story	8.9	17.8	37.2	74.5	7.34	14.7	54.9	109.8	22.9	45.8

Table D.2 Vertical characteristic of elastomeric bearings for 3-story frame

S	K_{eff} (kips/in)		Q_d (kips/in)		K_d (kips/in)		F_y (kips)		K_u (kips/in)	
	exterior	interior	exterior	interior	exterior	interior	exterior	interior	exterior	interior
30	66744	133434	111	222	55095	110145	163	327	171585	343032
28	58141	116236	99	198	47994	95949	146	292	149470	298819
25	46350	92663	93	186	38260	76490	137	273	119156	238216
22	35893	71758	80	160	29629	59234	118	235	92275	184475
20	29664	59304	74	148	24487	48953	109	218	76260	152459
17	21432	42847	77	153	17692	35369	113	226	55098	110151
15	16686	33359	74	149	13774	27536	109	219	42896	85758
12	10679	21349	75	149	8815	17623	110	220	27454	54885
10	7416	14826	71	141	6122	12238	104	208	19065	38115
9	6007	12009	66	132	4959	9913	97	195	15443	30873
8	4746	9489	62	124	3918	7833	91	182	12202	24393
7	3634	7265	60	121	3000	5997	89	178	9342	18676
6	2670	5337	65	129	2204	4406	95	190	6863	13721
5	1854	3707	58	115	1530	3060	85	170	4766	9529
4	1187	2372	54	108	979	1958	80	159	3050	6098
3	667	1334	51	103	551	1101	76	152	1716	3430
2	297	593	41	83	245	490	61	122	763	1525
1	74	148	28	56	61	122	41	82	191	381

Table D.3 Vertical characteristic of elastomeric bearings for 9-story frame

S	K_{eff} (kips/in)		Q_d (kips/in)		K_d (kips/in)		F_y (kips)		K_u (kips/in)	
	exterior	interior	exterior	interior	exterior	interior	exterior	interior	exterior	interior
30	48060	96120	529	1057	39672	79344	778	1557	123552	247105
28	41866	83731	474	947	34559	69117	698	1395	107628	215256
25	33375	66750	389	777	27550	55100	572	1145	85800	171601
22	25846	51691	300	600	21335	42669	442	884	66444	132888
20	21360	42720	263	526	17632	35264	388	775	54912	109824
17	15433	30865	198	396	12739	25478	291	583	39674	79348
15	12015	24030	166	332	9918	19836	244	489	30888	61776
12	7690	15379	142	284	6348	12695	209	418	19768	39537
10	5340	10680	148	296	4408	8816	218	437	13728	27456
9	4325	8651	145	290	3570	7141	214	428	11120	22239
8	3418	6835	133	265	2821	5642	195	391	8786	17572
7	2617	5233	123	246	2160	4320	181	363	6727	13453
6	1922	3845	117	234	1587	3174	173	345	4942	9884
5	1335	2670	114	229	1102	2204	168	337	3432	6864
4	854	1709	117	234	705	1411	172	344	2196	4393
3	481	961	89	179	397	793	132	263	1236	2471
2	214	427	56	112	176	353	83	165	549	1098
1	53	107	38	77	44	88	57	113	137	275

Appendix E

Viscous dampers properties

Table E.1 below provides information about the damping coefficient (c) for individual dampers corresponding to various damping ratio (10% and 20%) for 3- and 9-story frames.

Table E.1 Damping coefficient values for 3 and 9-story frame

S	3-story		9-story	
	c (kips-sec/in)		c (kips-sec/in)	
	ξ = 10%	ξ = 20%	ξ = 10%	ξ = 20%
30	117	234	146	292
28	109	218	136	272
25	97	195	121	243
22	86	171	107	214
20	78	156	97	194
17	66	133	83	165
15	58	117	73	146
12	47	94	58	117
10	39	78	49	97
9	35	70	44	87
8	31	62	39	78
7	27	55	34	68
6	23	47	29	58
5	19	39	24	49
4	16	31	19	39
3	12	23	15	29
2	8	16	10	19
1	4	8	5	10

Appendix F

Fragility curves

Tables F.1 to F.3 provide information to construct fragility curves for minor damage state, Tables F.4 to F.6 provide information to construct fragility curves for moderate damage state, and Table F.7 to F.9 provide information to construct fragility curves for major damage state.

F.1 Minor damage state

Table F.1 Badillo data for minor damage probability of failure

	Probability of failure (%)					
PVFA(g) / PHFA(g)	0	0.735	0.853	0.941	1.02	1.1
0	0	0	0	0	0	50
0.781	0	0				
0.969	0		50			
1.14	17			100	100	100
1.51	33			100	100	100
2	83			100	100	100

Table F.2 Interpolation data for PHFA = 0.05g

	Probability of failure (%)					
PVFA(g) / PHFA(g)	0	0.735	0.853	0.941	1.1	1.44
0.05	0	0	3	4	52	100

Table F.3 Interpolation data for PHFA = 0.85g

	Probability of failure (%)					
PVFA(g) / PHFA(g)	0	0.735	0.853	0.941	1.1	1.15
0.85	0	0	44	75	87	100

F.2 Moderate damage state

Table F.4 Badillo data for moderate damage probability of failure

Probability of failure (%)						
PVFA(g) / PHFA(g)	0	0.735	0.853	0.941	1.02	1.1
0	0	0	0	0	0	0
0.781	0	0	0	0		
0.969	0	0	0	0		
1.14	0	0	0	0		
1.51	0				67	
2	0					100

Table F.5 Interpolation data for PHFA = 0.05g

Probability of failure (%)						
PVFA(g) / PHFA(g)	0.853	0.941	1.02	1.1	2.92	4.89
0.05	0	0	2	3	50	100

Table F.6 Interpolation data for PHFA = 0.85g

Probability of failure (%)						
PVFA(g) / PHFA(g)	0.853	0.735	0.853	0.941	1.1	1.15
0.85	0	0	44	75	87	100

F.3 Major damage state

Table F.7 Badillo data for moderate damage probability of failure

Probability of failure (%)						
PVFA(g) / PHFA(g)	0	0.735	0.853	0.941	1.02	1.1
0	0	0	0	0	0	0
0.781	0	0	0	0		
0.969	0	0	0	0		
1.14	0	0	0	0		
1.51	0				0	
2	0					17

Table F.8 Interpolation data for PHFA = 0.05g

Probability of failure (%)						
PVFA(g) / PHFA(g)	0.853	0.941	1.02	1.1	2.92	4.89
0.85	0	0	0	0	0	0

Table F.9 Interpolation data for PHFA = 0.85g

Probability of failure (%)						
PVFA(g) / PHFA(g)	0.941	1.02	1.1	1.31	1.59	2.16
0.85	0	0	7	25	50	100

Appendix G

Column isolators

Similar to elastomeric bearings, column isolators were assumed to have bi-linear vertical force-deformation behavior to account for rubber inherent damping. 5 percent inherent damping in vertical direction was chosen to represent moderate damping rubber bearings. Tables G.1 and G.2 below provide information to construct column isolators at different floor level for 3- and 9-story frames.

A sample calculation to design exterior column isolators for 3-story frame

The vertical load demand is the sum of dead load and live load:

$P_D + P_L = 56\,\text{kips}$

Assuming static pressure $p = 0.5\,\text{ksi}$ and shape factor $S = 4$

$$A = \frac{W}{p} = \frac{56}{0.5} = 112\,\text{in}^2$$

Calculate diameter *D* of column isolator:

$D = 11.9\,\text{in}$

Calculate height of a single rubber layer (t_r):

$$t_r = \frac{D}{4S} = \frac{11.9}{4 \times 4} = 0.75\,\text{in}$$

Using trial and error to find the maximum number of rubber of layers (n) corresponding to lowest vertical stiffness and still satisfy stability requirement $P_{cro} \geq 3(P_D + P_L)$:

With $n = 5$: $P_{cro} = 153 \leq 3(P_D + P_L) = 168$ (not satisfied)

With $n = 4$: $P_{cro} = 193 \geq 3(P_D + P_L) = 168$ (accepted)

Total height of the rubber layer:

$T_r = t_r \times n = 0.75 \times 4 = 3\,\text{in}$

Calculate vertical stiffness for column isolator:

$$K_v = 6S^2 \frac{GA}{T_r} = 6 \times 4^2 \times \frac{0.1 \times 112}{3} = 360\,\text{kips/in}$$

Table G.1 Physical properties of column isolators for 3-story frame

Floor	Vertical load demand (kips)		Diameter (in)		No. of Rubber layers n		S		P_{cro} (kips)	
	exterior	interior	exterior	interior	exterior	interior	exterior	interior	exterior	interior
2	56	112	11.9	16.9	4	4	4	4	193	386

Table G.2 Vertical characteristic of column isolators for 3-story frame

Floor	Max vertical displacement (in)	Q_d (kips/in)		K_d (kips/in)		F_y (kips)		K_v (kips/in)	
		exterior	interior	exterior	interior	exterior	interior	exterior	interior
2	0.4	13	18	329	465	26	36	360	509

Table G.3 Physical properties of column isolators for 9-story frame

Floor	Vertical load demand (kips)		Diameter (in)		No. of Rubber layers n		S		P_{cro} (kips)	
	exterior	interior	exterior	interior	exterior	interior	exterior	interior	exterior	interior
2	253	506	24.2	34.2	12	12	7	7	764	1530
5	155	309	18.6	24.4	7	7	5	5	473	945
8	56	112	11.9	16.9	4	4	4	4	193	386

Table G.4 Vertical characteristic of column isolators for 9-story frame

Floor	Max vertical displacement (in)	Q_d (kips/in)		K_d (kips/in)		F_y (kips)		K_v (kips/in)	
		exterior	interior	exterior	interior	exterior	interior	exterior	interior
2	0.54	61	86	1190	1683	125	176	1304	1844
5	0.65	38	54	611	862	78	110	669	944
8	0.48	15	21	329	465	31	43	360	509

Appendix H

Vertical periods of 3- and 9-story frame

	Fundamental vertical periods (s)	
	3-story frame	9-story frame
Fixed-base	0.037	0.086

S	Fundamental vertical periods (s)			
	3-story frame		9-story frame	
	Base-isolated	Column isolators	Base-isolated	Column isolators
30	0.039	0.138	0.089	0.23
28	0.040	0.138	0.089	0.23
25	0.041	0.138	0.091	0.23
22	0.043	0.138	0.092	0.23
20	0.045	0.138	0.095	0.23
17	0.051	0.138	0.100	0.23
15	0.057	0.138	0.107	0.23
12	0.070	0.138	0.126	0.23
10	0.084	0.138	0.148	0.23
9	0.093	0.138	0.163	0.234
8	0.104	0.141	0.182	0.236
7	0.119	0.142	0.207	0.239
6	0.138	0.145	0.241	0.244
5	0.166	0.152	0.288	0.255
4	0.207	0.173	0.359	0.285
3	0.275	0.222	0.478	0.356
2	0.413	0.323	0.715	0.519
1	0.900	0.645	1.430	1.02